Cancer Research

Macrophage-Derived Neuropilin-2 Exhibits Novel Tumor-Promoting Functions

Sohini Roy[1,2], Arup K. Bag[1,2], Samikshan Dutta[1,2], Navatha Shree Polavaram[1,2], Ridwan Islam[1,2], Samuel Schellenburg[3], Jasjit Banwait[4], Chittibabu Guda[4], Sophia Ran[5], Michael A. Hollingsworth[1,2,6,7], Rakesh K. Singh[6], James E. Talmadge[6], Michael H. Muders[3,8], Surinder K. Batra[1,2,7], and Kaustubh Datta[1,2]

Abstract

Tumor-associated macrophages (TAM) are causally associated with tumorigenesis as well as regulation of antitumor immune responses and have emerged as potential immunotherapeutic targets. Recent evidence suggests TAM phagocytose apoptotic tumor cells within the tumor microenvironment through efferocytosis in an immunologically silent manner, thus maintaining an immunosuppressed microenvironment. The signal transduction pathways coupling efferocytosis and immunosuppression are not well known. Neuropilin-2 (NRP2) is a member of the membrane-associated neuropilin family and has been reported in different immune cells but is poorly characterized. In this study, we show that NRP2 is expressed during macrophage differentiation, is induced by tumor cells, and regulates phagocytosis in macrophages. Furthermore, NRP2 in TAM promoted efferocytosis and facilitated tumor growth. Deletion of NRP2 from TAM impaired the clearance of apoptotic tumor cells and increased secondary necrosis within tumors. This resulted in a break in the immune tolerance and reinitiated antitumor immune responses, characterized by robust infiltration of $CD8^+$ T and natural killer cells. This result suggests NRP2 may act as a molecular mediator that connects efferocytosis and immune suppression. Deletion of NRP2 in TAM downregulated several immunosuppressive and tumor-promoting genes and upregulated immunostimulatory genes in the myeloid compartment. Taken together, our study demonstrates that TAM-derived NRP2 plays a crucial role in tumor promotion through efferocytosis, opening the enticing option for the development of effective immunotherapy targeting TAM.

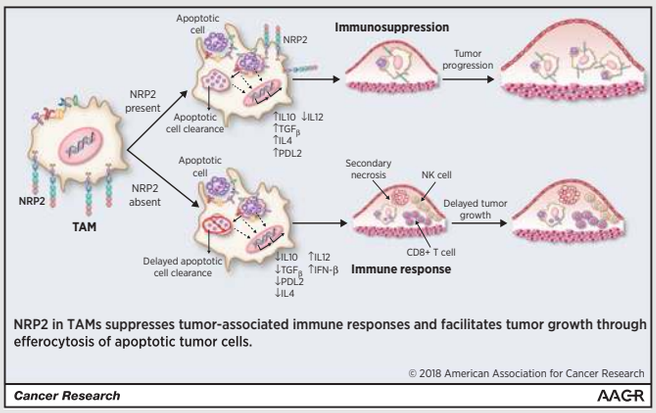

NRP2 in TAMs suppresses tumor-associated immune responses and facilitates tumor growth through efferocytosis of apoptotic tumor cells.

Cancer Research AACR

Significance: Neuropilin-2 in macrophages promotes tumor growth by regulating efferocytosis of apoptotic tumor cells and orchestrating immune suppression.

Graphical Abstract: http://cancerres.aacrjournals.org/content/canres/78/19/5600/F1.large.jpg. *Cancer Res; 78(19); 5600–17. ©2018 AACR.*

Introduction

Macrophages are multifaceted, highly plastic hematopoietic cells and extremely diverse in their functions. They are mononuclear phagocytes that maintain tissue homeostasis by clearing erythrocytes, apoptotic cells, and cellular debris (1, 2). They can also act as immune effector cells and bridge the innate and adaptive arms of the immune responses. Based on the nature of signals macrophages are exposed to in the tissue, they can either

[1]Department of Biochemistry and Molecular Biology, University of Nebraska Medical Center, Omaha, Nebraska. [2]Fred and Pamela Buffet Cancer Center at University of Nebraska Medical Center, Omaha, Nebraska. [3]Institute of Pathology, University Hospital Carl Gustav Carus, University of Technology, Dresden, Germany. [4]Department of Genetics, Cell Biology and Anatomy, University of Nebraska Medical Center, Omaha, Nebraska. [5]Department of Medical Microbiology, Immunology and Cell Biology, Southern Illinois University School of Medicine, Springfield, Illinois. [6]Department of Microbiology and Pathology, University of Nebraska Medical Center, Omaha, Nebraska. [7]Eppley Institute for Research in Cancer, University of Nebraska Medical Center, Omaha, Nebraska. [8]Rudolf Becker Laboratory for Prostate Cancer Research, Center of Pathology, University of Bonn Medical Center, Bonn, Germany.

Note: Supplementary data for this article are available at Cancer Research Online (http://cancerres.aacrjournals.org/).

Corresponding Author: Kaustubh Datta, University of Nebraska Medical Center, Fred and Pamela Buffet Cancer Center, Room# BCC 6.12.390, 985870 Nebraska Medical Center, Omaha, NE 68198. Phone: 402-559-7404; Fax: 402-559-6650; E-mail: kaustubh.datta@unmc.edu; and Michael H. Muders, Rudolf Becker Laboratory at the Biomedical Center (BMZ), Institute for Pathology, University of Bonn Medical Center, Sigmund-Freud-Strasse 25, D-53127 Bonn, Germany. Phone: 49-0-228-287-19397; E-mail: michael.muders@ukbonn.de

doi: 10.1158/0008-5472.CAN-18-0562

differentiate to classic type or alternative type macrophages and undergo profound changes in gene signature that we commonly refer to as "macrophage polarization." The classic type may arise following exposure to GM-CSF or Toll-like receptor (TLR) ligands such as LPS and IFN-γ and mediates resistance against pathogens, produces immunostimulatory factors (IL12), and is antitumorigenic. The alternatively activated type, which exists in many varieties, such as M2a, M2b, or M2c, due to their stimulation by different extracellular signals (such as M-CSF, IL4, IL13, IL10, and glucocorticoids) is collectively immunosuppressive in nature, upregulate the expression of CD163, CD206, IL10, IL4, TGFβ, and other anti-inflammatory cytokines to blunt T-cell responses (2, 3). Macrophages have also been causally associated with tumorigenesis and various stages of tumor progression and metastasis. High infiltration of tumor-associated macrophages (TAM) is a predictor of poor clinical outcome in various cancers (4, 5). Within the tumor, TAM behavior is dictated by microenvironment-derived factors that potentially suppress antitumor immune responses and actively promote disease progression. TAMs exhibit complex molecular profile(s), resembling more of the alternatively activated type macrophages, and actively suppress antitumor immune responses. Therefore, understanding the origin and the mechanistic functioning of TAMs and molecular approaches to reeducate them toward a cytotoxic and immunostimulatory phenotype is important for developing anticancer therapy.

Efferocytosis is a strictly orchestrated process where phagocytes, such as macrophages, recognize, engulf, and clear apoptotic cells in an immunologically silent manner. In adult humans, one million cells undergo apoptosis per second as part of the regular turnover process (6, 7). The apoptotic cellular debris is as efficiently removed as it is generated, to avoid inappropriately evoking the adaptive immune responses. If apoptotic cells are not engulfed, they release their cellular contents as secondary necrosis, and this results in aberrant immune responses by exposure to self-antigens and a break in tolerance (8–13). Efferocytosis reprograms macrophages toward an anti-inflammatory phenotype, suppressing the production of inflammatory cytokines, such as IL12, TNFα, and IL1, and upregulating the levels of immunosuppressive cytokines, such as TGFβ and IL10 (14, 15). Both TGFβ and IL10 are potent in dampening effector helper T-cell response by stimulating regulatory T cells and T helper 2 cells (16). The role of efferocytosis in cancer has remained elusive. However, there are now several examples to indicate that the nonimmunogenic properties of efferocytosis that prevail under normal homeostasis conditions can be mimicked by malignant cells to create an environment of immunosuppression in the TME. In the tumor microenvironment, TAMs show increased efferocytosis of apoptotic tumor cells, which also facilitates immune tolerance by rendering the former more protumorigenic and increase the risk for metastasis (17–19). A protumoral role of efferocytosis was also observed where tumor progression was dampened following genetic deletion of the efferocytosis receptor MerTK (20). $MerTK^{-/-}$ $CD11b^{+}$ cells isolated from the tumors showed signs of immune activation, characterized by elevated expression of IL12 and reduced expression of the immunosuppressive cytokines such as IL10. In a separate study, dendritic cells with increasing efferocytic activity, because of their exposure to liposomes containing the well-known "eat me" signal phosphatidylserine (PS), failed to upregulate several costimulatory molecules and had diminished capacity to produce IL12 and activate T-cell responses (21). Efferocytosis of apoptotic tumor cells by TAMs also facilitates prostate cancer metastases (22). However, the molecules that couple the two pathways, efferocytosis and immune modulation, are still not well known.

Neuropilins (NRP) are multifunctional cell surface, nontyrosine kinase receptors that are expressed in all vertebrates and highly conserved across species. NRPs have been associated with cellular processes such as development, axonal guidance, angiogenesis, immunity, bone homeostasis as well as pathologic conditions like cancer. The two major isoforms of NRPs, NRP1 and NRP2, are transmembrane glycoproteins comprising of an N-terminal extracellular domain followed by a transmembrane region and a short cytosolic tail of 43 to 44 amino acids. There is some degree of amino acid identities among the domains between NRP1 and NRP2, suggesting their overlapping cellular functions. However, functions unique to each isoform have also been reported. Work over the past few years has documented a role for NRPs in the immune responses. NRP1 is important for the formation of immune synapse between dendritic cells and T lymphocytes. It is also considered to be a marker for murine regulatory T cells (Treg) where its expression correlates with immunosuppression. NRP1 is also reported to be expressed in tumor-infiltrating macrophages and microglia (23–26). Recently, Miyauchi and colleagues reported a tumor-promoting function of NRP1 in glioma-infiltrating microglia and macrophages. Their study revealed that either genetic ablation or pharmacologic manipulation of NRP1 expression in microglia or bone marrow–derived macrophages (BMDM) arrested glioma progression and increased antitumorigenic polarization in the microglia and macrophages (25, 26). NRP2, on the other hand, is much less characterized in the immune cell compartments. It is constitutively expressed in human thymic developing DP ($CD4^{+}CD8^{+}$) T cells. NRP2 is also detected in dendritic cells and microglia where it is posttranslationally modified by polysialylation (27).

In the present study, we sought to determine the role of NRP2 in macrophages and its implication in tumor progression. We detected expression of NRP2 in macrophages present in pancreatic cancer (PDAC) tissues. Our results indicate a novel function of NRP2 in promoting efferocytosis of apoptotic cells by macrophages and that, in its absence, the clearance of the apoptotic cell corpse is delayed. We also found that NRP2 deletion in macrophages resulted in increased infiltration of cytotoxic $CD8^{+}$ T lymphocytes and natural killer (NK) cells into the tumor and thus slowed pancreatic tumor growth. This could be attributable to delayed clearance of dying tumor cells by NRP2-deleted macrophages, which resulted in secondary necrosis leading to an antitumor immune response. Further, NRP2 deletion in TAMs has a direct effect on their ability to express several immunosuppressive and checkpoint inhibitor genes, such as *IL10*, *TGFβ*, *IL4*, *MMP*s, and *PDL2* as well as immunostimulatory genes such as *IL12* and thereby provides an additional mechanism of antitumor immune response. Together, we believe, our observations will affect the therapeutic approaches for targeting TAMs in the treatment of cancer.

Materials and Methods

Antibodies used

NRP2 (CST 3366 for mouse, R&D AF2215 for human), CD8 (CST 98941), CD68 (eBioscience 14-0681-82), F4/80

(eBioscience 14-4801-82), CD31 (ab28364), Rab5 (ab13253), Rab7 (ab50533), Rho GDI (Santa Cruz Biotechnology, sc373724), β-actin (Cell Signaling Technology, 4970), Hsc 70 (Santa Cruz Biotechnology, sc 7298), α,β tubulin (Cell Signaling Technology 2148), CD69 (BioLegend 104502, clone H1.2F3), NK1.1 (abcam, 25026), and CD 163 594 PE-dazzle (BioLegend 333623, clone GHI/61).

Animals

Animals were housed at the University of Nebraska Medical Center (UNMC) facility. All animal experiments were performed according to the animal care guidelines, as approved and enforced by the Institutional Animal Care and Use Committee at the University of Nebraska Medical Center. The $NRP2^{flox/flox}$ mouse was developed by and a kind gift from Dr. Peter Mombaerts, Max Planck Research Unit for Neurogenetics, Frankfurt am Main, Germany (28). These mice were later bred to pure C57BL/6 background. The FVB-Tg(Csf1r-Mer-iCre-Mer)1Jwp/J mice (developed by Dr. Jeffrey W. Pollard, Albert Einstein College of Medicine, Bronx, NY) were purchased from The Jackson Laboratories. These transgenic mice express a Cre recombinase/mutant murine estrogen receptor double-fusion protein under the control of the mouse Csf1r promoter. Tamoxifen-inducible Cre activity was detected in bone marrow–derived as well as yolk sac macrophages. CSF1R-iCre mice were bred with $NRP2^{f/f}$ mice to obtain CSF1R-iCre;$NRP2^{f/f}$ where NRP2 can be conditionally deleted from the myeloid lineage following administration of tamoxifen intraperitoneally or adding (Z)-4-HudroxyTamoxifen into the cell culture medium. Genotyping was performed following Jackson Laboratories standard protocol.

Cell culture and generation of human peripheral blood monocyte-derived macrophages and murine BMDMs

Monocytes isolated from the peripheral blood of unidentified healthy human donors were obtained from the Elutriation Core Facility at the University of Nebraska Medical Center. Cells obtained were >97% pure. Monocytes were then cultured at 37°C with 5% CO_2 in RPMI 1640 containing 10% fetal bovine serum, 2 mmol/L glutamine, 100 μg/mL streptomycin, and 100 U/mL penicillin for the indicated time points, with either 100 ng/mL GM-CSF or M-CSF. For generation of mouse macrophages, bone marrow from either C57BL/6 or CSF1R-iCre;$NRP2^{f/f}$ mice was flushed from the femurs and tibia with ice-cold PBS using a 25-gauge 30cc needle. Red blood cells (RBC) were removed using erythrocyte lysis buffer. Cells were resuspended in αMEM media containing 10% fetal bovine serum, 2 mmol/L glutamine, 100 μg/mL streptomycin, and 100 U/mL penicillin and differentiated using either 50 ng/mL murine recombinant GM-CSF or 100 ng/mL M-CSF for indicated time points. For some experiments, to knock out NRP2, (Z)-4-hydroxytamoxifen (1 mmol/L stock in methanol) was added into the culture media at a concentration of 0.3 μmol/L every alternate day for 3 to 5 days.

Panc-1 cells were purchased from ATCC. UNKC-6141 (derived from spontaneous pancreatic tumors arising in mice harboring a mutation in $K\text{-}Ras^{G12D}$ in the pancreas) cells were generated by Dr. Surinder K. Batra, University of Nebraska Medical Center, and were a kind gift to us from his laboratory. All these cell lines were maintained in DMEM containing 10% fetal bovine serum, 2 mmol/L glutamine, 100 μg/mL streptomycin, and 100 U/mL penicillin at 37°C with 5% CO_2. For generation of conditioned media, cells were plated in 75 mm^2 tissue culture flasks and allowed to grow until 75% confluency. The complete media were then removed, and cells were washed twice with PBS without calcium or magnesium and replaced with only DMEM for 48 hours. The conditioned media were then collected, centrifuged at 1000 rpm for 5 minutes, strained through 0.22-μm filter, and kept at −80°C until use.

Jurkat cells were purchased from ATCC and cultured in RPMI-1640 medium containing 2 mmol/L L-glutamine, 10 mmol/L HEPES, 1 mmol/L sodium pyruvate, 4500 mg/L glucose, and 1500 mg/L sodium bicarbonate, 10% FBS, 100 μg/mL streptomycin, and 100 U/mL penicillin at 37°C and 5% CO_2.

Where mentioned, peripheral blood-derived human monocyte (PBMC) and BMDM were treated with conditioned media (50% v/v) collected from pancreatic cancer cell line Panc-1 (ATCC) and UNKC-6141 cell lines, respectively, for the indicated periods of time.

Procurement of PDAC patient tissue and mouse pancreatic cancer tissue

Tissues from patients with pancreatic cancer but no previous history of treatment were procured from the Rapid Autopsy Pancreatic Program (RAPP) at the University of Nebraska Medical Center.

Nucleofection of human monocytes or macrophages

siRNA transfection in human monocytes or macrophages was performed using the Human Monocyte Nucleofection Kit (Lonza, VPA-1007) following the manufacturer's protocol. siNRP2 or Scrambled antisense RNA (25 nmol/L) was used. Where mentioned, 40 nmol/L siNRP1 RNA was used. Cells were analyzed or subjected to any assay 48 to 72 hours after siRNA transfection.

Immunoblot analysis

Briefly, cells were washed with ice-cold PBS followed by lysis with CHAPS lysis buffer (150 mmol/L KCl, 50 mmol/L HEPES (pH 7.4), 0.1% CHAPS, 2 mmol/L EDTA, 20 μg/mL leupeptin, 10 μg/mL aprotinin, 5 mmol/L DTT, 1 mmol/L PMSF and Halt protease and phosphatase inhibitor cocktail) on ice. Cells were gently scraped using cell scraper and sonicated on ice. Supernatant was separated by cold centrifugation (13,000 rpm for 5 minutes) and total protein was estimated using the Bradford method (Bio-Rad). SDS sample buffer was added, and the sampled were heated at 95°C for 8 minutes. The whole-cell extracts were next run on 4% to 20% Mini-PROTEAN TGX Gel (Bio-Rad) and transferred to polyvinylidene difluoride (PVDF) membrane (Life Technologies). The membrane was then blocked in either 5% nonfat dry milk or 5% bovine albumin serum (BSA) in 1× TBST (1× Tris Buffered Saline, 0.1% Tween-20) and then incubated overnight in 1× PBS containing appropriate dilution of primary antibodies overnight at 4°C with continuous shaking at low speed. The next day, the membrane was washed with 1× TBST and then incubated for 1 hour in 1× TBST containing appropriate dilution of horseradish peroxidase-conjugated secondary antibody (Santa Cruz Biotechnology) with continuous shaking at low speed. The membranes were washed in 1× TBST and the protein bands were detected using SuperSignal West Femto Maximum Sensitivity Substrate (Pierce). For successive immunoblots, membranes were stripped in Stripping Buffer (Thermo Fisher Scientific) for 20 minutes, reblocked in 1× TBST

containing either 5% BSA or 5% nonfat dry milk, and probed as mentioned before.

Phagocytosis and pulse and chase *in vitro* clearance assay

For phagocytosis assay, the pHrodo Red *E. coli* BioParticles Conjugate or pH-insensitive *E. coli* bioparticles (red or green) suspension was prepared following the manufacturer's protocol. An optimized dose of 65 μg/mL bioparticles was used for phagocytosis.

Human PBMC-derived macrophages or murine BMDM were grown in two-well chambers as described. Human MDM were subjected to nucleofection on day 5 to knock down NRP2, and the assay was performed on day 7. Before the assay, cells were washed twice with 1× Dulbecco's phosphate-buffered saline (PBS). The fluorescent *E. coli* particles were then added at a concentration of 65 μg/mL and incubated at 37°C for the indicated periods of time to allow adequate particle internalization. Where mentioned, pHrodo red and pH-insensitive *E. coli* bioparticles were added simultaneously. Under conditions where we simultaneously added pHrodo red and pH-insensitive green *E. coli* bioparticles, an optimized dose of 33 μg/mL of either type was used. Phagocytosis was arrested by placing the cells on ice and washing vigorously 3 to 5 times with 1× PBS to remove the excess particles. Cells were then fixed with 4% paraformaldehyde at 4°C for 20 minutes and washed with PBS to remove the excess fixative. Nuclei were stained using the nuclear dye Hoechst in PBS and analyzed by either Zeiss LSM 800 with Airyscan or Zeiss 710 Confocal Laser Scanning Microscope at UNMC confocal core facility, and data were analyzed and processed with the Zeiss Zen 2010 software. All confocal data were quantified using ImageJ software, and graphical illustrations were made using GraphPad Prism software as mentioned later.

For an *in vitro* clearance assay, BMDMs were grown in two-well chambers as described earlier. On day of the experiment, cells were washed twice with 1× PBS and added 500 μL of Opti-MEM media per well. pHrodo red *E. coli* or zymosan bioparticles were added at a concentration of 65 μg/mL for indicated time (pulse) to allow their internalization. Uptake was stopped by adding ice-cold PBS. Cells were washed vigorously with PBS (×3) to remove any *E. coli* or zymosan particle that was not taken up or loosely adhered to cell surface. Fresh complete α-MEM media were added, and the cells were monitored at different time points (chase). At each time point, chambers were taken out, cells vigorously washed with PBS (×5) and fixed with 4% PFA for 20 minutes at 4°C, nuclei stained with Hoechst and analyzed using confocal microscopy as described earlier.

Efferocytosis assay

Apoptosis was induced in Jurkat or UNKC-6141 cells using 50 and 75 μmol/L etoposide (Abcam), respectively, and kept overnight at 37°C and 5% CO_2 for 12 hours. This treatment routinely yielded 80% to 90% apoptotic cells. Cells were centrifuged at 2,000 rpm for 10 minutes, and the pellet was washed twice with PBS. The cells were incubated with pHrodo Red succinimidyl ester (Thermo Scientific) following the manufacturer's instructions. Cells were centrifuged at 2,000 rpm for 10 minutes. The cell pellet was washed twice with 1× PBS and resuspended in Opti-MEM medium (Gibco). Mouse BMDM were plated in two-well chambers and grown in the presence of M-CSF or conditioned media (CM) collected from UNKC-6141 cells. (Z)-4-Hydroxytamoxifen was added to knock out NRP2 as described earlier. Apoptotic Jurkat or UNKC-6141 cells were added to the macrophages (10:1 target-to-effector ratio) for 1 hour (pulse) at 37°C. Uptake was stopped by adding ice-cold PBS; cells were vigorously washed with ice-cold PBS to remove any cell that was not phagocytized or remained loosely bound to the cell surface. Fresh complete α-MEM media were added to the cells, and the clearance of apoptotic cells was monitored for the indicated time (chase). Nuclei were counterstained using Hoechst for 5 minutes and analyzed using confocal microscopy as mentioned earlier.

IHC and immunofluorescence

IHC and immunofluorescence staining on histologic sections were performed using the following procedure: slides containing tissue sections (4 μm thick) were kept on heat block at 58°C for 2 hours. They were then rehydrated in a sequential passage of solutions starting with xylene for 20 minutes, 100% ethanol for 15 minutes, 95%, 90%, 80%, 75%, 50%, and 20% ethanol for 5 minutes each followed by immersion in double distilled water for 10 minutes. For IHC only, slides were next immersed in 3% hydrogen peroxide (H_2O_2) in methanol for 1 hour at room temperature followed by incubation in double distilled water for 5 minutes. Antigen retrieval was performed using Dako antigen retrieval solution (either pH9 or pH6, depending on the antigen of interest). The antigen unmasking solution was first preheated at a high temperature in the microwave until boiling and then the slides were immersed into it and boiled on a 98°C water bath for 45 minutes. Following this, the slides were gradually allowed to cool to room temperature and washed with 1× PBS. Slides were then blocked with 5% goat serum in 1× PBS containing 0.2% saponin at 4°C for 1 hour and incubated overnight with primary antibody in PBS containing 0.2% saponin and 3% BSA at 4°C. Biotinylated antibodies (IHC) or 1:500 for fluorophore-conjugated antibodies (IF) was added. For IHC staining, slides were next washed with 1× TBS and then incubated with avidin–biotin complex for 40 minutes at room temperature, following the manufacturer's instructions and added diaminobenzidine solution containing 0.3% H_2O_2 as a substrate for peroxidase (Dako) until the desired staining intensity was developed. Hematoxylin was used to counter staining. Slides were dehydrated by gradual passage of slides from double distilled water to xylene in a reverse order mentioned earlier for rehydration of slides and mounted with Permount and covered with glass cover slips. The whole slides were next digitally scanned at Tissue Science Facility, UNMC. For IF, following incubation with secondary antibody cells were washed and mounted with Vectashield mounting media containing DAPI (Vector Laboratories).

Snap-frozen tissues were fixed in 10% neutral buffered formalin for 20 minutes, followed by permeabilization in 2% TritonX-100 in PBS for 30 minutes. Slides were blocked in 5% goat serum in 0.2% TritonX-100 containing PBS for 1 hour and then incubated with primary antibody for 1 hour. Slides were washed in 1× TBS and secondary antibody added. DAPI was used to stain the nuclei.

For monolayer culture, immunofluorescence staining was performed as described: briefly, cells were grown on poly-D-lysine–coated coverslips (BD Biosciences) for indicated periods of time before fixation and analysis by confocal microscopy. Cells were rinsed with PBS (Invitrogen), followed by fixation with ice-cold

4% paraformaldehyde at 4°C for 20 minutes. Cells were then washed with PBS and blocked using 1% BSA and 0.2% saponin in PBS for 1 hour at 4°C in a moist chamber. The slides were then incubated overnight in the same blocking buffer containing appropriate concentration of primary antibodies at 4°C. The next day, the coverslips were carefully washed in 1× PBS and fluorescent conjugated antibodies added (1:200) in 1× PBS containing 1% BSA and 0.2% saponin at 4°C. Slides were washed and mounted with Vectashield mounting media containing DAPI (Vector Laboratories).

Slides were viewed using either Zeiss LSM 800 with Airyscan or Zeiss 710 Confocal Laser Scanning Microscope at UNMC confocal core facility, and data were analyzed and processed with the Zeiss Zen 2010 software. All confocal data were quantified using ImageJ software and graphical illustrations made using GraphPad Prism software.

Flow-cytometric analysis

Human peripheral blood-derived monocytes and murine bone marrow–derived cells (BMDC) were treated with either GM-CSF, M-CSF, or CM from pancreatic cancer cell lines for 7 days as described earlier. Cells were then harvested, washed, and resuspended in FACS buffer (ice-cold PBS containing 10% BSA and 1% sodium azide) at a concentration of 3×10^6 cells/mL. Cells were incubated with CD163-PE 594 dazzle antibody and kept for 1 hour at 4°C in the dark. Following this, cells were washed 3× at 400 × *g* for 5 minutes and resuspended in FACS buffer at a concentration of 3×10^6 cells/mL and immediately analyzed. LIVE/DEAD Fixable Blue Dead Cell Stain (Thermo Fisher Scientific) was added to quantify the viability of the cells.

Subcutaneous tumor implantation

500,000 or 2×10^6 UNKC-6141 cells were mixed with equal volume of Matrigel (without growth factors) and implanted subcutaneously into the right flank of animals. For our studies, mice were divided into two groups, control and test ($n = 3$ or 5). To deplete NRP2 from the macrophages, the test group was injected with tamoxifen intraperitoneally (75 mg/kg body weight from a 20 mg/mL stock in corn oil) every day until the endpoint of the experiment. The control group received corn oil as a vehicle control. The tumor growth was manually monitored regularly using digital slide calipers and weight of the mice recorded. Once the endpoint of the experiment was reached, mice were euthanized by CO_2 asphyxiation following Institutional Animal Care and Use Committee protocol and tumors harvested. Harvested tumors were washed gently in ice-cold PBS, transferred to new tubes containing PBS and kept on ice. Tumors were fixed in 10% formaldehyde overnight and transferred to 70% ethanol and given to Tissue Science Facility at UNMC for paraffin embedding, sectioning (4 μm) and hematoxylin and eosin staining.

Isolation of CD11b$^+$ cells from subcutaneous tumors

Subcutaneous mouse tumors were generated as mentioned earlier. The harvested tumors were kept in ice-cold RPMI media on ice and cut into small pieces. The digestion media were added (RPMI media containing the following: 10 U/mL collagenase I, 400 U/mL collagenase IV, 30 U/mL DNAse I—all diluted in HBSS) and kept at 37°C for 30 minutes. Following this, the tumor pieces were crushed with the plunger of a 10 mL syringe, 5 mL RPMI media were added and homogenized well. The tumor suspension was filtered by passing through a 70-μm nylon gauze, the suspension centrifuged at 450 × *g* for 6 minutes at 4°C; the pellet was resuspended in 2 mL erythrocyte lysis buffer to remove the RBCs. The tubes were allowed to stand for 2 minutes at room temperature, neutralized by the addition of 12 mL of RPMI media, passed through a sterile 70-μm nylon gauze and centrifuged again at 450 × *g* for 6 minutes at 4°C. The pellet was resuspended in Lymphoprep solution at a concentration of 1×10^7 to 2×10^7 cells/mL and transferred to fresh tubes. To this was added 6 mL RPMI media very cautiously to obtain a two-phase gradient. The gradients were centrifuged at 800 × *g* for 30 minutes at room temperature without acceleration or break. The interphase (enriched in myeloid cells and lymphocytes as well as the upper layer containing the RPMI media were collected into fresh tubes without disturbing the Lymphoprep layer. The cells were washed once with MACS buffer, centrifuged at 800 × *g* for 5 minutes at 4°C and the supernatant was discarded. The cell pellet was finally resuspended in MACS buffer at a concentration of 10^8 cell/mL. TAMs were isolated using CD11b magnetic beads and LS columns (both from Miltenyi Biotech) following the manufacturer's instructions. The CD11b$^+$ myeloid cells were arrested in the columns and collected for isolation of RNA and RNA-seq analysis.

Visualization of monosodium urate crystals using polarizing microscope

Frozen tumor tissue sections (4 μm) were fixed with neutral buffered formalin (10%) for 20 minutes, washed in PBS, and mounted with Consulmount mounting media. MSU crystals were visualized using Velocity software and polarizing filters at 5× magnification. The intensity of MSU crystals per field was quantified using ImageJ software and represented as a scatter plot.

Transcriptome analysis using RNA-seq and bioinformatics analysis

CD11b$^+$ cells were isolated from subcutaneous tumors. RNA was isolated from the control and test group with $n = 3$ animals contributing to each pool. This was done in order to obtain sufficient amount of RNA. RNA-seq service was obtained from Kelvin Chan and his team at Seqmatic. Extracted RNA was quality controlled with Agilent TapeStation RNA ScreenTape. The RNA integrity number value of the control sample was 9.1 and that of the test was 9.4. Libraries were prepared using Illumina TruSeq Stranded mRNA kit. A paired end read 2 × 75 bp sequencing run of RNA libraries was performed using the Illumina NextSeq 500 instrument. For analysis, raw reads were demultiplexed by barcode and output into FASTQ format. Cutadapt was used to filter out adapter sequences and low-quality bases. Filtered sequence reads were aligned to mouse reference genome grcm38 using HISAT2 aligner. Reads mapping to exon regions as defined by Ensembl gene annotations were counted using FeatureCounts. Data analysis was performed with the help of Seqmatic and the Bioinformatics Core at UNMC. Raw data was submitted to Gene Expression Omnibus (GEO accession number GSE118501). Genes with a cutoff value log fold change (±1) were selected, and those with zero counts in either control or test samples were eliminated for stringency. The Ingenuity Pathway Knowledge Base (IPA) was used to identify the enriched cellular and molecular functions among the differentially expressed transcripts in the two samples. The Database for Annotation, Visualization and Integrated Discovery (DAVID), The Gene Ontology Project, Kyoto Encyclopedia of Genes and Genomes (KEGG) pathway were used

and extensive literature reviewed to annotate differentially regulated transcripts with a GO designation. Among the enriched functional annotation clusters, we selected representative clusters (as mentioned in the Results section) to analyze the effect of NRP2 deletion on phagocytosis, macrophage phenotype, and secretion of chemokines and cytokines as well as interaction between macrophages and leucocytes/lymphocytes.

Statistical analyses

All the graphical illustrations statistical tests were performed using Prism-6 software (GraphPad software, Inc.). All data reported in graphs are expressed as mean ± standard error of mean (SEM) unless otherwise mentioned and were compared using unpaired Student *t* test; *P* values were considered statistically significant when less than 0.05. All experiments were repeated at least 3 times unless specified. *, $P < 0.05$; **, $P < 0.005$; ***, $P < 0.0005$. ns, not significant.

Results

NRP2 is induced during differentiation of monocytes to macrophages and is expressed by TAMs

To evaluate the expression pattern of NRP2 in macrophages in response to differentiation stimuli, we obtained freshly isolated PBMCs from the Elutriation Core Facility. Immunoblot analysis revealed freshly isolated monocytes do not express NRP2 protein at a detectable level; however, its expression was induced within 24 to 72 hours following stimulation with M-CSF (Fig. 1A). NRP2 expression was maintained in the similar level when M-CSF–induced macrophages were further treated with IL4, IL10, and IL13 to promote differentiation to different alternative subtypes (Supplementary Fig. S1A). We corroborated our observations in human macrophages using BMDMs isolated from C57BL/6 mice. Immunoblot analysis revealed a similar expression pattern for NRP2 as in human monocytes/macrophages (Fig. 1B). Flow-cytometric analysis of human macrophages revealed 93.33% of M-CSF–induced macrophages expressed CD163, a marker for alternatively activated macrophages, whereas 2.73% of GM-CSF–treated macrophages were positive for CD163 (Supplementary Fig. S2A). Similarly, confocal microscopy showed a majority of $CD163^{+}$ human and mouse macrophages expressed NRP2 following M-CSF treatment (Supplementary Fig. S2B). Further, M-CSF treatment induced the expression of immunosuppressive genes such as *IL10* and *MMP-9* but not inflammatory genes such as *IL12b* (Supplementary Fig. S2C). NRP2 was similarly upregulated in both human and mouse macrophages following its differentiation with GM-CSF (Supplementary Fig. S1B and S1C). TAMs are abundantly present

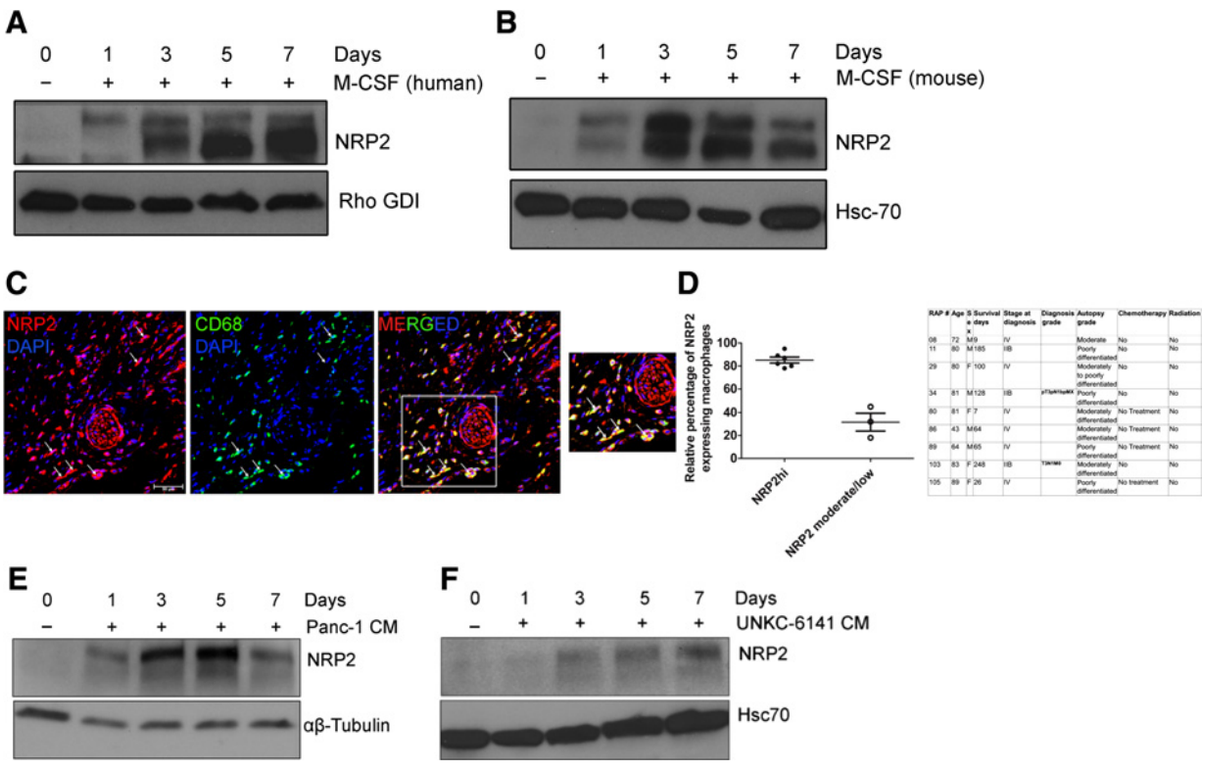

RAP #	Age	S	Survival e days	Stage at diagnosis	Diagnosis grade	Autopsy grade	Chemotherapy	Radiation
08	72	M	9	IV		Moderate	No	No
11	80	M	185	IIB		Poorly differentiated	No	No
29	80	F	100	IV		Moderately to poorly differentiated	No	No
34	81	M	128	IIB	xTubHistMX	Poorly differentiated	No	No
80	81	F	7	IV		Moderately differentiated	No Treatment	No
86	43	M	64	IV		Moderately differentiated	No Treatment	No
89	64	M	65	IV		Poorly differentiated	No Treatment	No
103	83	F	248	IIB	TUM1MS	Moderately differentiated	No	No
105	89	F	26	IV		Poorly differentiated	No treatment	No

Figure 1.

Expression of NRP2 in macrophages. **A** and **B,** NRP2 expression in freshly isolated human monocytes and bone marrow cells from C57BL/6 mice differentiated to macrophages with M-CSF. **C,** Representative confocal image showing the presence of NRP2-expressing $CD68^{+}$ TAMs in human PDAC tissue. The first panel shows only NRP2-positive cells (red). The second panel shows $CD68^{+}$ macrophages (green). The third panel represents merged image, showing $NRP2^{+}CD68^{+}$ macrophage in the tumor. Scale bar, 20 μm. The inset shows a magnified image of part of the tissue. DAPI was used to stain the nucleus. **D,** Graphical representation showing relative abundance of $NRP2^{+}$ macrophages in a cohort of treatment-naïve PDAC tissues derived from RAPP. The table shows details of patient tissues procured. **E** and **F,** Immunoblot analyses showing NRP2 expression in human and mouse macrophages differentiated with pancreatic cancer cell line–derived conditioned medium (CM) from Panc-1 or UNKC-6141 cells, respectively, *in vitro*.

in solid tumor microenvironment and are causally associated with various aspects of tumor progression, immune evasion, metastasis, and therapy resistance (5). The infiltration of TAMs correlates with disease stage and worse prognosis in a wide variety of malignancies, including PDAC (4, 29, 30). TAMs have been typically shown to more resemble M-CSF–induced alternatively activated macrophages. To evaluate whether TAMs in PDAC express NRP2 in treatment-naïve conditions, we obtained tissue sections from a cohort of 10 patients with treatment-naïve pancreatic cancer from the Rapid Autopsy Program at University of Nebraska Medical Center. Details about the disease stage and grade of the tissues are provided in Fig. 1. Our data revealed that 6 samples had high number of $NRP2^+$ TAMs (on average 85% macrophages expressed NRP2) and 3 showed moderate to low number (on average 30%) of $NRP2^+$ TAMs. One sample showed very scarce infiltration of $CD68^+$ cells (not shown in graph; Fig. 1C and D). However, currently we do not know how the function and immunophenotype of $NRP2^-$ TAMs differ from that of $NRP2^+$ TAMs in PDAC. It is also difficult to conclude from our small tissue cohort if NRP2 expression in TAMs correlates with stage and grade of the disease, metastatic potential, or overall survival of the patients. These aspects of NRP2 expression in TAMs merit further investigation using a bigger tissue cohort. Next, we differentiated human PBMCs with CM from a human PDAC cell line, Panc-1. Immunoblot analyses showed a strong induction of NRP2 expression in the macrophages within 24 hours of treatment with CM (Fig. 1E). Similarly, treatment of mouse BMDMs with CM from UNKC-6141 cells induced NRP2 expression in the macrophages (Fig. 1F). Flow-cytometric analysis with CM-treated human macrophages revealed 94.9% cells expressed CD163, indicating Panc-1 CM drives the macrophages toward an alternatively activated phenotype (Supplementary Fig. S2D). Confocal microscopy revealed that a majority of either Panc-1 or UNKC-6141 CM-treated macrophages that expressed CD163 were also positive for NRP2 expression (Supplementary Fig. S2E and S2F). Also, Panc-1 and UNKC-6141 CM induced the expression of immunosuppressive and wound healing genes but not immunostimulatory genes in human macrophages and BMDMs (Supplementary Fig. S2C and S2G), indicating an alternative type activation. Overall, these data indicate NRP2 is not detected in monocytes or bone marrow precursors; however, it is expressed in macrophages under GM-CSF, M-CSF, as well as cancer cell–derived CM-induced conditions.

NRP2 regulates phagosome maturation and degradation in macrophages without significantly affecting the uptake of phagocytic cargo

Phagocytosis is one of the key functions of macrophages and important for maintenance of physiologic homeostasis as well as microbial clearance during infections (31). We wanted to test whether NRP2 regulates the phagocytic activity of macrophages. For this, we performed a pulse and chase phagocytosis assay using pH-sensitive red fluorophore-tagged *E. coli* bioparticles (pHrodo red). The *E. coli* bioparticles are nonfluorescent at neutral pH; however, their fluorescence intensity increases with an increase in acidity of the vesicle they are localized in. Following engulfment, phagocytic cargo remains in nascent early phagosomes of higher pH, which sequentially mature to late phagosomes, becoming more and more acidic and finally fuse with the lysosomes for degradation and clearance. Therefore, a bright red fluorescence dot in the cell indicates a mature phagocytic vesicle containing the *E. coli*, which has or is going to be fused with lysosomes and thus can indicate an active phagocytic process. We have developed a transgenic mouse model by breeding $NRP2^{f/f}$ with CSF-1R-iCRE mice. In the resultant CSF1R-iCre;$NRP2^{f/f}$ mice, NRP2 can be selectively and conditionally deleted genetically from the monocytes/macrophages following administration of tamoxifen or addition of (Z)-4-hydroxytamoxifen into cell culture medium. For the phagocytosis assay, M-CSF–treated BMDMs from CSF1R-iCre;$NRP2^{f/f}$ mice were challenged with pHrodo red *E. coli* bioparticles for 15 minutes (pulse) and then excess *E. coli* bioparticles that were either not phagocytized or remained loosely bound to macrophages were washed off. Next, the phagosome maturation, degradation, and clearance of the already phagocytized bioparticles from the cells were monitored at 15 minutes, 45 minutes, 1.5 hours, 2 hours, and 4 hours (chase) using confocal microscopy. Images revealed that in the control macrophages, starting from 0 minutes up to 2 hours chase, there was a gradual increase in the intensity and number of red fluorescence, indicating gradual maturation and fusion of the *E. coli* containing phagosomes with lysosomes. Interestingly, at 4-hour chase, there was once again a decrease in the intensity of the visible red puncta, suggesting degradation of the phagocytized *E. coli* bioparticles (Fig. 2A). This means that the engulfed *E. coli* bioparticles containing phagosomes matured into late phagosomes or phagolysosomes and then the bioparticles underwent degradation in the control macrophages. In contrast, in the NRP2-deleted macrophages, we observed that until 90 minutes (chase), there was no significant visible red fluorescence indicating a delayed maturation of the *E. coli* bioparticles. However, from the 120-minute chase time period, we did observe some phagosomes maturation in the NRP2-deleted cells; however, the red intensity of these did not reach the maximal level as seen in WT macrophages. This indicated that the phagosome maturation in NRP2-deleted macrophages was significantly delayed compared with the WT macrophages. At 4-hour chase, higher value of total cellular fluorescence in the NRP2-deleted cells in comparison to the control macrophages at the same time point indicated that phagosomes have now started maturing in the former, whereas the bioparticles are almost degraded at this time in the control cells (Fig. 2B). This indicated that in control macrophages, phagosomes containing *E. coli* bioparticles matured and fused with lysosomes and degraded the phagocytic cargo, whereas in the absence of NRP2, there was a defect in maturation of phagosomes and degradation of *E. coli* bioparticles. Overall, these data suggested that NRP2 regulates phagosome maturation and therefore degradation and clearance of engulfed cargo.

Following uptake of *E. coli* bioparticles, the TLR4 pathway is activated. Therefore, we wanted to determine whether NRP2 selectively regulates TLR4-mediated phagosome maturation and degradation or whether it can regulate cellular mediators common to other types of phagosome maturation and degradation. To test this, we repeated the pulse and chase experiment using pHrodo zymosan particles (a yeast component that activates the TLR2 pathway) that are nonfluorescent at neutral pH but show bright red fluorescence in the acidic late phagosomes or phagolysosomes. Depending on the cargo, phagosome maturation and eventual clearance may follow different kinetics. Based on our preliminary observations, the degradation of internalized

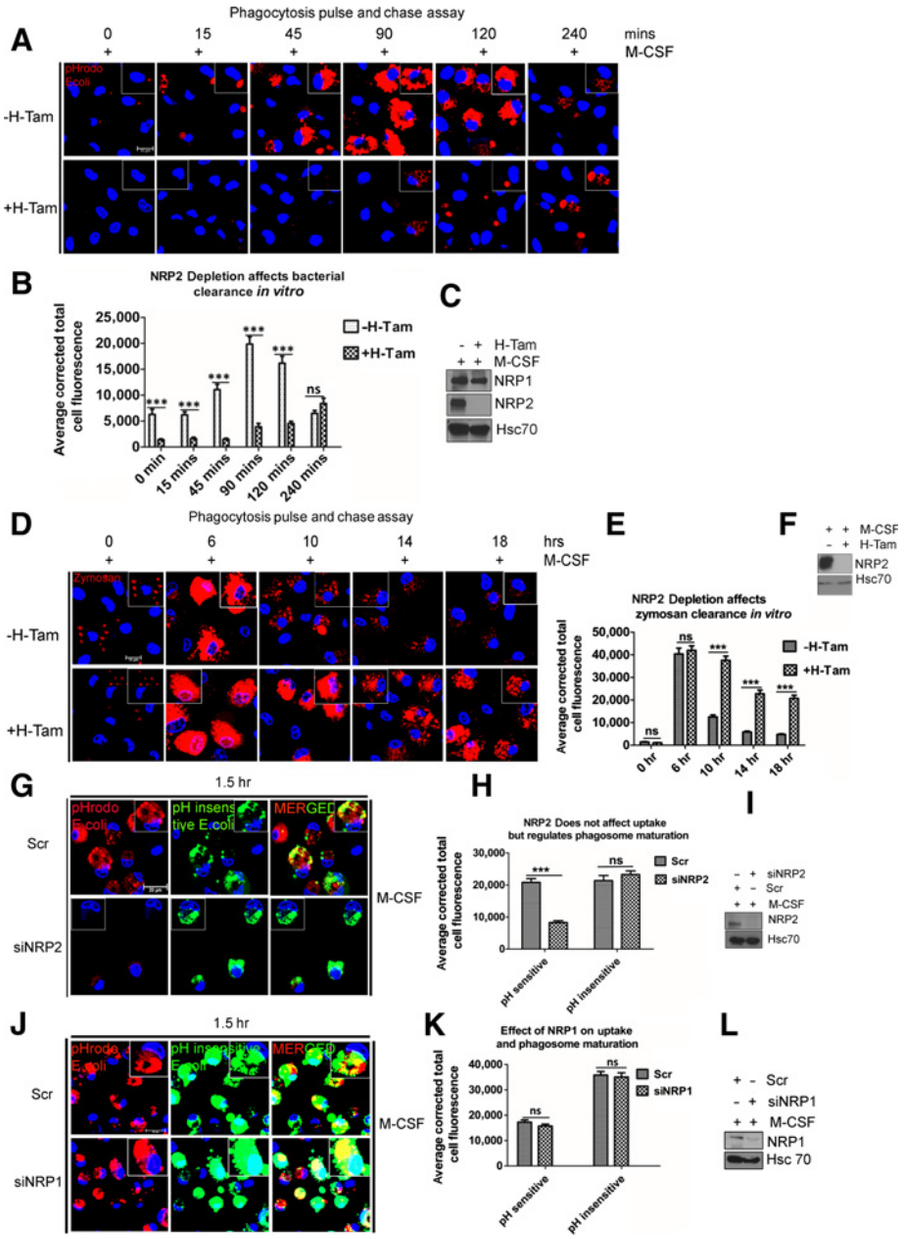

Figure 2.

NRP2 regulates phagosome maturation without affecting uptake of phagocytic cargo. **A,** BMDMs from NRP2$^{f/f}$CSF1R-iCre mice were assessed for phagosome maturation and degradation of internalized *E. coli* bioparticles at time = 0, 15, 45, 90, 120, and 240 minutes. Scale bars, 10 μm. Magnified images within the inset show the phagosomes containing *E. coli* particles. **B,** Phagosome maturation and degradation of bioparticles were assessed as corrected total cell fluorescence using ImageJ software at times indicated on the graph abscissa and are represented in bar graphs as mean ± SEM. **C, F,** and **I,** Western Blots showing knockout or deletion of NRP2 for each experiment. **C,** NRP1 protein level following NRP2 knockout in macrophages. **D,** M-CSF–treated BMDMs from NRP2$^{f/f}$CSF1R-iCre mice were analyzed for phagosome maturation and degradation of internalized zymosan particles at time = 0, 6, 10, 14, and 18 hours. Scale bars, 10 μm. Magnified images within the inset show the phagosomes containing zymosan particles. **E,** Phagosome maturation and degradation of zymosan particles were scored as corrected total cell fluorescence using ImageJ software at times indicated and are represented in bar graph as mean ± SEM. **G,** Phagocytosis assay for assessing the ability of human macrophages to uptake *E. coli* bioparticles (green) and phagosome maturation (red) following NRP2 knockdown. The first column shows phagosome maturation (red) in the scr (top)- and siNRP2-treated (bottom) cells. The second column indicates the uptake efficiency (green) in the scr (top)- and siNRP2-treated (bottom) cells. The third column represents merged images showing the role of NRP2 on uptake and phagosome maturation. Scale bars, 20 μm. Single cell magnified within the boxed region shows green or red *E. coli* particle. **H,** Uptake efficiency was measured as green cellular fluorescence, whereas the intensity of red fluorescence indicated phagosome maturation. Results are represented graphically, values as mean ± SEM. DAPI was used for staining the nucleus. **J,** Phagocytosis assay was done to show the effect of NRP1 depletion on cargo uptake (green) as well as phagosome maturation (red) in human macrophages. Insets show a magnified image of cell containing bacteria. Scale bars, 10 μm. **K,** Phagosome maturation and uptake efficiency in the presence and absence of NRP1 were quantified as in **H** and are represented graphically as mean ± SEM. **L,** Western blot showing NRP1 knockdown. ***, $P < 0.0005$; ns, not significant.

zymosan particle containing phagosomes was monitored at 6, 10, 14, and 18 hours (chase). After 15-minute pulse (0 hours' time point of chase), both the control and NRP2-deleted macrophages showed similar number of zymosan-containing phagosomes. At 6 hours, there was an increased red fluorescence in both the control and NRP2-deleted cells. This possibly indicated maturation of zymosan-containing phagosomes in control and NRP2 knocked out cells and that in case of zymosan, NRP2 is not involved in the regulation of early stages of maturation. However, at 10, 14, and 18 hours, the control macrophages gradually degraded and cleared the zymosan particles, as evident from the decreased intensity of visible red puncti structures of the zymosan particles. Interestingly, NRP2 knockout macrophages showed a significantly delayed degradation and clearance of zymosan particles. This was evident from the bright red fluorescence and bigger size of the zymosan particles that persisted within the cells, even at 18 hours, when the control cells had efficiently degraded individual particles (Fig. 2D and E). To further confirm whether NRP2 is involved in the uptake process, we repeated the phagocytosis uptake assay with BMDM using *E. coli* bioparticles tagged with a pH-insensitive red fluorophore that shows uniform fluorescence intensity irrespective of the pH of the phagosome they are localized in. Therefore, the visible red puncta as observed using this dye indicate the uptake efficiency of the macrophages. We observed a modest difference in uptake efficiency in NRP2-deleted cells (Supplementary Fig. S3A). The slight decrease in the uptake efficiency in the absence of NRP2 can arise as a secondary effect of delayed downstream maturation and degradation of the internalized cargo, which subsequently dampened the uptake.

To confirm if NRP2 plays a similar role in phagocytosis in human macrophages, M-CSF–treated macrophages were challenged with pHrodo red and pH-insensitive green *E. coli* bioparticles simultaneously for 1.5 hours. This experimental approach enabled us to simultaneously test the ability of the macrophages to mature the phagosomes (red) as well as their uptake efficiency (green) in the presence and absence of NRP2. Quantification of the average total cell fluorescence revealed a significant decrease in the intensity of red puncta, indicating a delayed phagosomal maturation in siNRP2–treated cells. However, the uptake efficiency in mock and siNRP2 treated macrophages were similar, as evident from the intensity of the green puncta (Fig. 2G and H). These data therefore confirmed that similar to mouse macrophages, NRP2 regulates phagosome maturation in human macrophages, without significantly affecting the uptake process. Because, during infection or injury, GM-CSF–induced inflammatory macrophages are predominantly found in tissues and phagocytose pathogens, we tested the role of NRP2 in phagocytosis in GM-CSF–treated human macrophages. Our results indicated a similar maturation defect with no significant effect on the uptake efficiency in the absence of NRP2 (Supplementary Fig. S3D and S3F). These data suggest that NRP2 regulates phagocytosis in macrophages through modulation of phagosome maturation.

NRP2 and NRP1 are both expressed in macrophages. Because of their structural similarity, both isoforms may have redundant as well as unique functions. Interestingly, the observed defect in phagosome maturation was more specific to the absence of NRP2 as we did not observe any significant difference in the phagosome maturation or uptake efficiency when NRP1 was knocked down in macrophages (Fig. 2J and K). Immunoblot analysis also did not reveal any change in NRP1 protein level following NRP2 deletion in BMDM, indicating further that our observation is possibly an NRP2-specific function (Fig. 2C). Additionally, we simultaneously knocked down NRP1 and NRP2 in human macrophages and repeated phagocytosis assay with pHrodo and pH-insensitive *E. coli* bioparticles. However, under our experimental conditions, we failed to observe any additive effect on cargo uptake or phagosome maturation in the absence of both NRP1 and NRP2 (Supplementary Fig. S3I and S3J). Nevertheless, with our experimental model, it is difficult to rule out the possibility that NRP1 may possibly regulate phagocytosis albeit with lesser efficiency. It is also possible that both NRP2 and NRP1 regulate nonoverlapping although essential functions for efficient phagocytic activity in macrophages, and the residual NRP1 present following siNRP1 treatment is sufficient to maintain the part of the function it regulates. This possibility will be tested in genetically engineered mouse system in our future studies.

NRP2 regulates early-to-late phagosome maturation

Nascent phagosome maturation occurs in a step-wise manner through sequential recruitment of Rab5 to the early phagosomes followed by Rab7 to the late phagosomes. To confirm our previous observations that NRP2 is involved in the regulation of phagosome maturation, we next assessed $Rab5^+$ early phagosomes and $Rab7^+$ late phagosomes in NRP2-proficient and -deficient cells. In NRP2 knocked down human macrophages, there was an increased accumulation of $Rab5^+$ early phagosomes and a concomitant decrease in the $Rab7^+$ late phagosomes (Fig. 3A). Similar observations were made in mouse BMDM following NRP2 knockout (Fig. 3D). Interestingly, total cellular protein level of Rab5 and Rab7 remained unchanged (Fig. 3C and F). Together, these data suggest that NRP2 regulates phagosome maturation in macrophages. Deletion or knockdown of NRP2 arrests phagosomes in the early stages and impairs their maturation to late phagosomes or phagolysosomes. Further, because we observed an increase in $Rab5^+$ vesicles in NRP2-depleted macrophages, it indicates NRP2 acts downstream of Rab5.

NRP2 in macrophages regulates efferocytosis of apoptotic cells

Macrophages efficiently phagocytose and clear apoptotic cells in tissues. This is indispensable for the maintenance of immunologic homeostasis. Impaired efferocytosis results in aberrant immune activation (32). Maturation of nascent efferosome (phagosome containing apoptotic debris) and subsequent degradation share similarity with classic phagocytosis. Both the pathways often hire similar family of effector molecules (6, 7, 33, 34). Our previous data suggested that NRP2 regulates phagosome maturation and the degradation of phagocytized cargo in macrophages. Using pHrodo *E. coli* bioparticles, we also observed a maturation defect in NRP2-deleted macrophages treated with cancer cell CM (Supplementary Fig. S4D and S4E). Based on these findings, we wanted to investigate the role of NRP2 in the clearance of dying cells by macrophages. To test this, BMDMs were challenged with apoptotic Jurkat cells and then monitored for their ability to degrade the internalized apoptotic cargo for up to 8 hours. Degradation was assessed from the loss of fluorescence and disappearance of

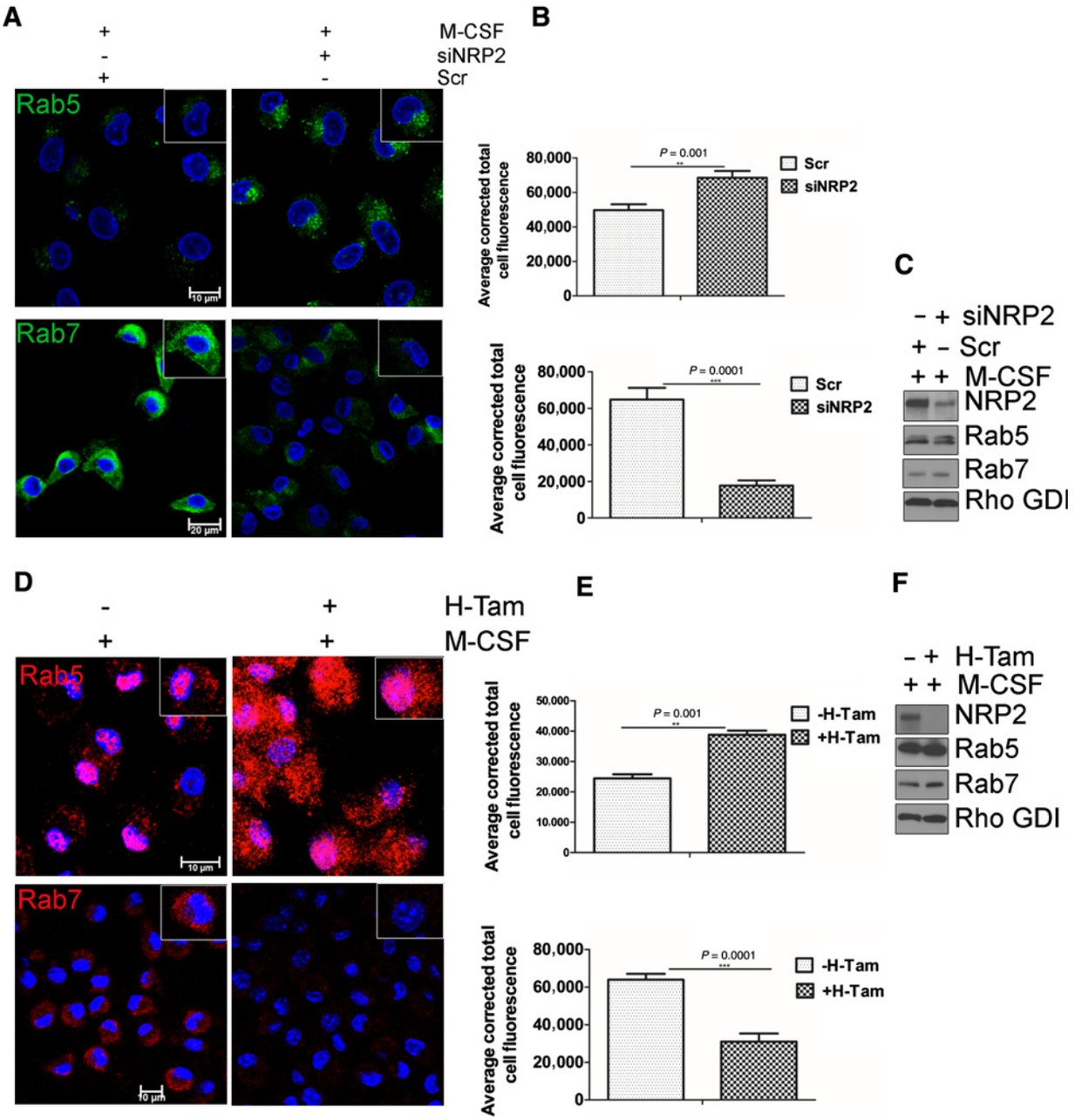

Figure 3.

Effect of NRP2 on early and late phagosomes. Knockdown or deletion of NRP2 inhibits maturation of early to late phagosomes in macrophages. **A,** Immunostaining of early and late phagosomal maturation markers in human macrophages following NRP2 knockdown. Top, early phagosome marker Rab5 (green). Scale bars, 10 μm. Bottom, representative of the late phagosomal marker Rab7 (green). Scale bars, 20 μm. Magnified images of individual cell are shown in the inset for each condition. **B,** Immunostaining data for Rab5 and Rab7 were quantified as cellular fluorescence using ImageJ software and are represented graphically. Top and bottom, graphical representation of Rab5 and Rab7, respectively, in the presence and absence of NRP2. **D,** Immunostaining of early and late phagosomal maturation markers in mouse BMDM following NRP2 deletion. Top and bottom, early phagosome marker Rab5 (red) and the late phagosomal marker Rab7 (red), respectively. Scale bars, 10 μm. The insets are magnified image of individual cell for each condition. **E,** Representative bar graphs showing quantification of Rab5 and Rab7 using ImageJ software. Top and bottom, changes in Rab5 and Rab7, respectively, following NRP2 deletion. All values are shown as mean ± SEM. DAPI was used for staining the nucleus. **C** and **F,** Western blot showing total cellular Rab5 and Rab7 in whole-cell lysates from human and mouse macrophages following knockdown or knockout of NRP2, respectively.

the apoptotic cells (red). At 2-hour chase, there was significant increase in the red fluorescence in both the control and NRP2 KO cells, indicating mature efferosomes. However, at 6 hours, there was a significant decrease in the red fluorescent intensity and disappearance of apoptotic cells in the control macrophages, indicating their degradation. In contrast, even after 8 hours, NRP2 KO cells exhibited significant delay in the clearance of apoptotic cell cargo (Fig. 4A and B). This was apparent from larger size of the cargo and higher amount of fluorescence that persisted in the cells even after 8 hours. Similar to our previous observation, NRP2 deletion did not result in the change in uptake efficiency of apoptotic cargo. No notable difference was observed when we quantified the average number of cells engulfed by macrophages at 0-hour chase (immediately after the incubation or uptake phase) following NRP2 deletion (Fig. 4B).

Recent studies have highlighted the importance of efferocytosis in tumor progression and metastasis (17, 20, 22). Infiltrating TAMs efficiently phagocytose and remove the dying cancer cells from the tumor milieu. This induces the expression of tumor-promoting immunosuppressive and wound-healing genes in TAMs and suppresses the antitumor immune responses, while actively supporting tumor growth. Based on our previous data that NRP2 deletion affects the clearance of apoptotic cells, we further wanted to investigate if NRP2 regulates the clearance of apoptotic debris by TAMs. Our preliminary observations revealed NRP2 was expressed by F4/80^{+} TAMs in subcutaneous mouse pancreatic cancer tissues (Supplementary Fig. S5A). To test the role of NRP2 in apoptotic cell clearance, UNKC-6141 CM-treated BMDMs from NRP2$^{f/f}$;CSF-1R-iCre mice were subjected to efferocytosis pulse and chase assay. At the beginning of chase, there was no significant difference in the intensity of red fluorescence in the control and NRP2 KO cells. At 2-hour chase, the intensity increased in the control and NRP2 KO macrophages, indicating the efferosomes are maturing and becoming acidic. However, at 6 and 12 hours of chase, there was a significant decrease in the intensity of red fluorescence as well as size of the internalized apoptotic debris in the control macrophages, suggesting efficient degradation and clearance of apoptotic cells. In contrast, the higher red fluorescent intensity in the NRP2 KO macrophages at the above-mentioned time points indicated a delayed clearance of apoptotic cargo in the absence of NRP2 (Fig. 4D and E). A similar

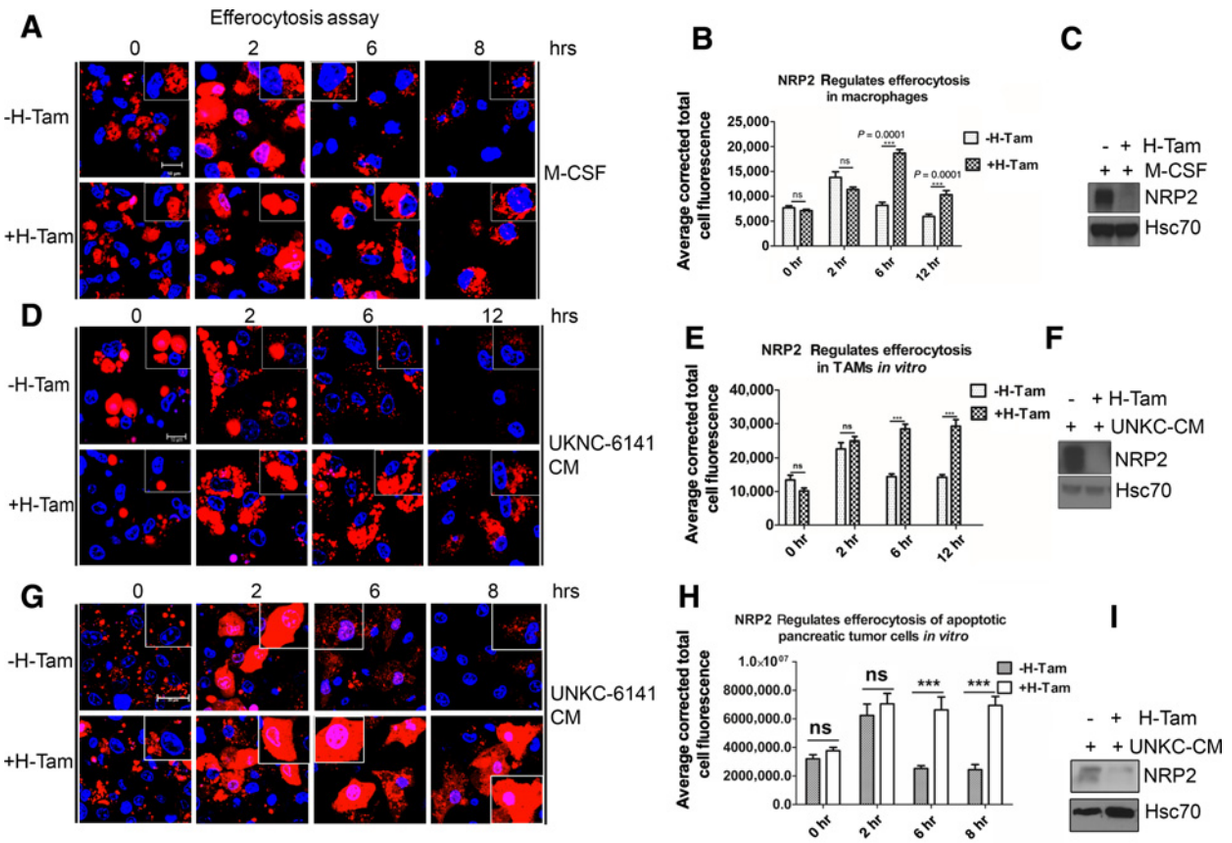

Figure 4.

NRP2 regulates efferocytosis of apoptotic cells by macrophages *in vitro*. Efferocytosis assay was done to assess the effect of NRP2 deletion on the ability of macrophages to degrade the apoptotic cells. **A**, **D**, and **G,** BMDM from NRP2$^{f/f}$CSF1R-iCre mice were treated with either M-CSF (**A**) or UNKC-6141 CM (**D** and **G**) and then assessed for degradation of internalized apoptotic Jurkat cells (**A** and **D**) or UNKC-6141 cells (**G**) at time points = 0, 2, 6, and 8 or 12 hours. Scale bars, 10 μm (**A** and **D**); 20 μm (**G**). Insets show single macrophage containing apoptotic cells. **B, E,** and **H,** Corrected total cellular fluorescence (red) was analyzed at the time points indicated using ImageJ software as a measure for efferosome maturation and degradation of the apoptotic cargo. Results are represented graphically as mean ± SEM. **C, F,** and **I,** Immunoblot$^{f/f}$ shows knockout of NRP2 for **A, D,** and **G**. DAPI was used for staining the nucleus. ***, $P < 0.0005$; ns, not significant.

defect in the degradation of phagocytized apoptotic UNKC-6141 cells was observed in NRP2 KO macrophages treated with CM derived from the same cell line (Fig. 4G and H). Overall, these results suggested that NRP2 regulates efferocytosis of apoptotic cells in macrophages, during physiologic homeostasis (M-CSF) as well as cancer cell CM-induced conditions.

NRP2 in macrophages affects tumor growth and antitumor adaptive immune response

Previous studies have demonstrated the tumor-promoting role of efferocytosis (17). That clearance of dying cells is an immunologically silent process is mimicked by cancer cells to promote disease progression and metastasis (17). To examine the role of macrophage NRP2-mediated efferocytosis on tumor growth, we used a subcutaneous pancreatic cancer mouse model where we implanted either 2×10^6 or 500,000 UNKC-6141 cells into the right flank of $NRP2^{f/f}$; CSF1R-iCre mice. Once the tumors became palpable, animals were randomly divided into control and test groups ($n = 3$ or 5). Tamoxifen was administered intraperitoneally to selectively knock out NRP2 from the macrophages. Tumors were regularly measured, and tumor growth was monitored over a period of 21, 25, or 15 days (Fig. 5A). Under all conditions, deletion of NRP2 in macrophages reduced the tumor size (Fig. 5C, E, and G) as well as the relative tumor volume (Fig. 5B). Importantly, tamoxifen administration into tumor-bearing Cre^- mice did not have any effect on tumor growth, although we observed a trend toward higher tumor volume in Cre^- animals that received tamoxifen compared with Cre^+ mice that did not receive tamoxifen (Fig. 5B). This suggests that the reduction in tumor growth we observed is because of deletion of NRP2 from macrophages. Although not statistically significant, we also observed a reduction in the weight of the tumors following NRP2 deletion in the macrophages (Supplementary Fig. S6A–S6C). Recent studies have shown that BMDMs are actively recruited to feed the pool of TAMs in tumors. To confirm that NRP2 was efficiently knocked out from TAMs, we isolated bone marrow from control and test animals and differentiated them to macrophages with M-CSF. Immunoblot analysis with lysates from BMDM as well as well as RNA-seq data from $CD11b^+$ myeloid cells isolated from tumors (mentioned later) indicated tamoxifen efficiently delete NRP2 not only from BMDM but

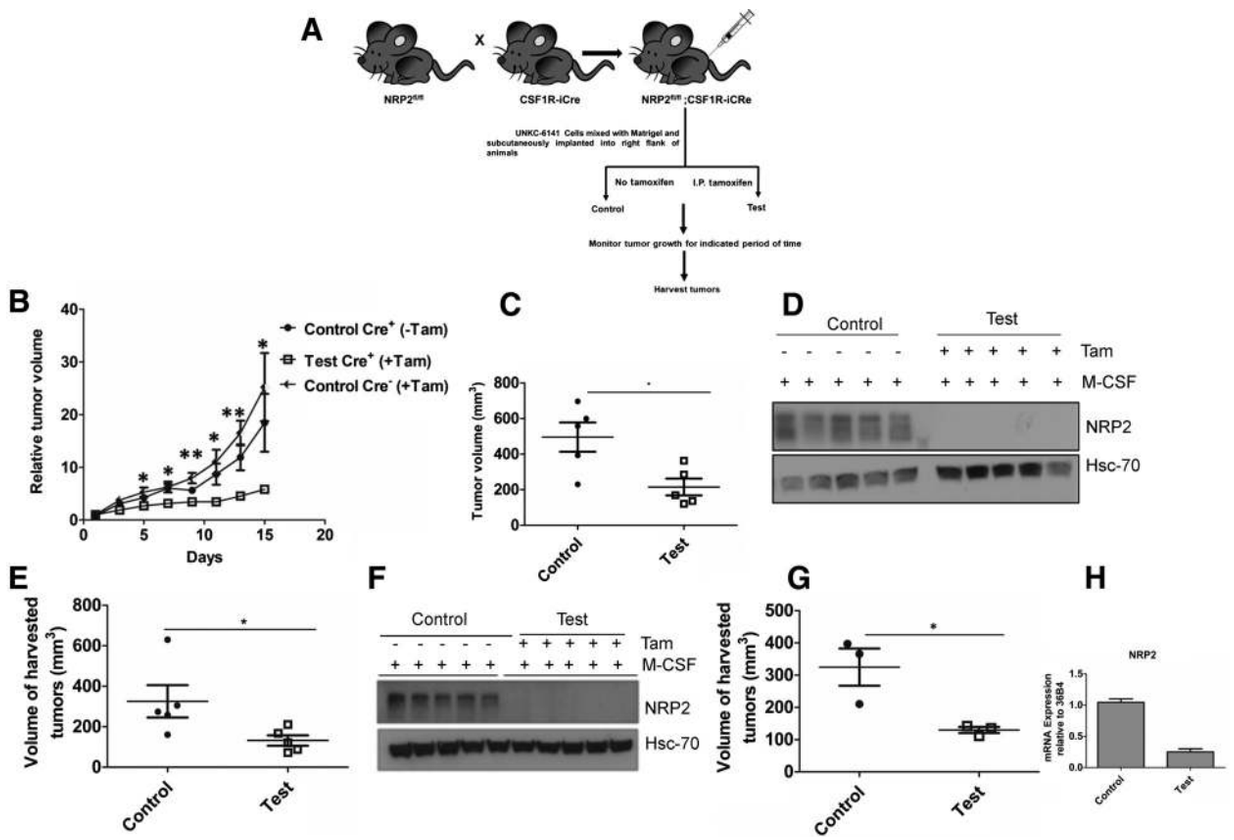

Figure 5.

NRP2 in macrophages affects tumor growth. **A,** Schematic diagram for subcutaneous tumor progression model. The 2×10^6 or 500,000 UNKC-6141 cells were subcutaneously implanted into $NRP2^{f/f}$CSF1R-iCre mice. Tumor progression was monitored for the indicated time periods. **B,** Graph showing relative tumor volume for control and test tumors (2×10^6 cells implanted). **C,** Scatter plot representation of the final volume of the harvested tumors (2×10^6 cells implanted). **D** and **F,** Immunoblot analysis showing efficient knockout of NRP2 from macrophages for experiment **B** and **E**. **E** and **G,** Graphical representation of final volume of harvested tumors ($n = 3$ or 5,500,000 cells implanted). **H,** RT-PCR showing efficient knockout of NRP2 from $CD11b^+$ myeloid cells isolated from test tumors for **G**. *, $P < 0.05$.

also from intratumoral macrophages (Fig. 5D, F, and H), suggesting the effect on tumor growth arises due to NRP2 deletion in macrophages. Further confocal staining indicated an efficient deletion of NRP2 from the intratumoral F4/80$^+$ macrophages, whereas NRP2 was still detected in surrounding tissue (Supplementary Fig. S7A). It has been reported that efferocytosis of apoptotic tumor cells has a protumorigenic effect on TAMs and blockade of this process may hinder tumor growth and metastasis (17). To assess if the decrease in tumor growth was due to inefficient efferocytosis by NRP2-deleted TAMs, TUNEL staining was performed. An increase in the number of necrotic foci in test tumors following NRP2 deletion from macrophages suggested apoptotic tumor cells were not efficiently removed and underwent secondary necrosis (Fig. 6A and B). Secondary necrotic cells release uric acid (derived from degradation of nuclear DNA) into the extracellular space, which then, in the presence of high sodium concentration, forms monosodium urate (MSU) crystals and can be visualized using a polarizing microscope. As hypothesized, we detected significantly higher amount of MSU crystal deposition in test tumors, indicating impaired efferocytosis and increased secondary necrosis in the tissues (Fig. 6C and D). NRP2 is well characterized for its role in migration. To test if the inefficient efferocytosis was a consequence of decreased recruitment of macrophages to the site of the tumor, we stained histologic sections of tumors with anti F4/80. Our data revealed no significant change in the average number of macrophages per field in control and test tumors, indicating NRP2 is dispensable for TAM recruitment (Fig. 6E and F). Therefore, we concluded that the increased accumulation of late apoptotic or necrotic cells in the tumor tissue was a consequence of dampened efferocytosis ability of NRP2 KO TAMs. Further, staining with anti-CD31 antibody revealed no significant difference in average vessel density between the control and test tumors, suggesting intratumoral angiogenesis was unaffected following NRP2 deletion in TAMs (Supplementary Fig. S7A and S7B).

Inefficient efferocytosis leads to secondary necrosis, which can activate adaptive immune response. Indeed, we observed a ~3-fold increase in intratumoral infiltration of cytotoxic CD8$^+$ T cells in the test tumors following NRP2 deletion. These data suggest NRP2 in macrophages suppress antitumor immune response and that its deletion in macrophages results in enhanced recruitment of CD8$^+$ T cells into the tumor (Fig. 6G and H). Staining with early activation marker CD69 indicated an active CD8 T-cell response following NRP2 deletion (Fig. 6I and J). Interestingly CD69 is also expressed by other immune cells, such as NK cells. Staining with NK cell marker NK1.1 revealed a significant increase in NK cell infiltration in test tumors following NRP2 deletion in macrophages (Fig. 6K). Overall, these data suggest a protumorigenic role of NRP2 in TAMs in suppression of antitumor adaptive immune response through efferocytosis of apoptotic tumor cells.

Transcriptome analysis from CD11b$^+$ myeloid cells by next-generation RNA-seq

Extensive efferocytic activity of macrophages present in tumor promotes M2 polarization. We therefore speculated that inhibition of efferocytic activity can directly affect the polarization of TAMs toward antitumorigenic macrophages. We isolated CD11b$^+$ myeloid cells from the control and test tumors and determined their polarization by analyzing gene expression using next-generation RNA-seq. Figure 7A shows the schematic diagram of the experiment. We considered transcripts that were differentially expressed more than 2-fold ($\log_2$ fold change 1) in either control or test sample and eliminated all transcripts with zero counts in either sample for stringency. After applying the cutoff, of the 3,616 differentially expressed genes, 1,567 genes were upregulated, whereas 2,049 genes were downregulated following NRP2 deletion. These differentially expressed transcripts were uploaded to the IPA database to identify the major enriched cellular and molecular functions in the absence of NRP2 in macrophages. We observed that pathways related to immune responses such as leucocyte extravasation signaling, role of cytokines in mediating communication between immune cells as well as phagosome formation were significantly affected. Some of the representative IPA pathways with gene enrichment and statistical significance are shown in Fig. 7B.

For the current study, we were mainly interested in understanding the intrinsic immune responsive gene signature changes occurring in the myeloid compartment as a consequence of impaired efferocytosis in the absence of NRP2 in macrophages. To gain a better understanding of the functional processes affected by NRP2 deletion, we determined the biological process gene ontological classification for each altered transcript using the DAVID and KEGG databases in combination with extensive review of the published literature. As with IPA analysis, using DAVID, we observed that genes related to immune response and leucocyte/lymphocyte regulation were abundantly regulated. Also, clusters comprising of genes functionally annotated to cytokine and chemokine signaling were enriched (Fig. 7C). Genes from IPA, KEGG, and DAVID clusters as well as from extensive review of the curated literature for T and NK cell–related immune responses, cytokine/chemokine signaling pathways, and phagocytosis and phagosome maturation were compiled and a unique gene list was created for each function and compared with our data set of 3,616 differentially regulated genes.

Our analysis from IPA software and DAVID and KEGG pathways (Fig. 7D) revealed many of the immunosuppressive genes and those associated with EMT and metastasis, such as *IL4*, *IL10* (3), *IL21R* (35), *IL33* (36), *IL34* (37), and *IL1β* (38, 39) were downregulated in the CD11b$^+$ myeloid cells following NRP2 deletion. MMPs are associated with cancer progression (40–42). Genes associated with ECM remodeling such as *MMP9*, *MMP13*, *MMP11*, *MMP23*, and *MMP25* were also downregulated following NRP2 deletion. Among the inflammatory genes, we observed an upregulation of *IFN-β1*, *IL12a*, *Gr-K*, and *Gr-F*. Further, by RT-PCR we validated the altered expression of *IL10*, *IL4 MMP9*, *MRC2*, checkpoint inhibitor such as *PDL2* and immunostimulatory gene such as *IL12a* in separate biological replicates (RNA pooled from $n = 3$ in either control or test groups; Fig. 7E). Macrophages also secrete TGFβ to suppress immune responses. It also acts as a strong inducer of tumor-promoting TAMs. Interestingly, RT-PCR revealed a significant downregulation of *TGFβ* in NRP2-deleted myeloid cells (Fig. 7E). These observations are in support of our hypothesis and indicate that NRP2 can act as a molecular mediator that can couple efferocytosis and immunosuppression in macrophages.

Overall, we believe that the components of the secondary necrotic cells along with altered expression of several cytokines, chemokines, and other signaling molecules in the myeloid compartment following NRP2 deletion in monocytes/

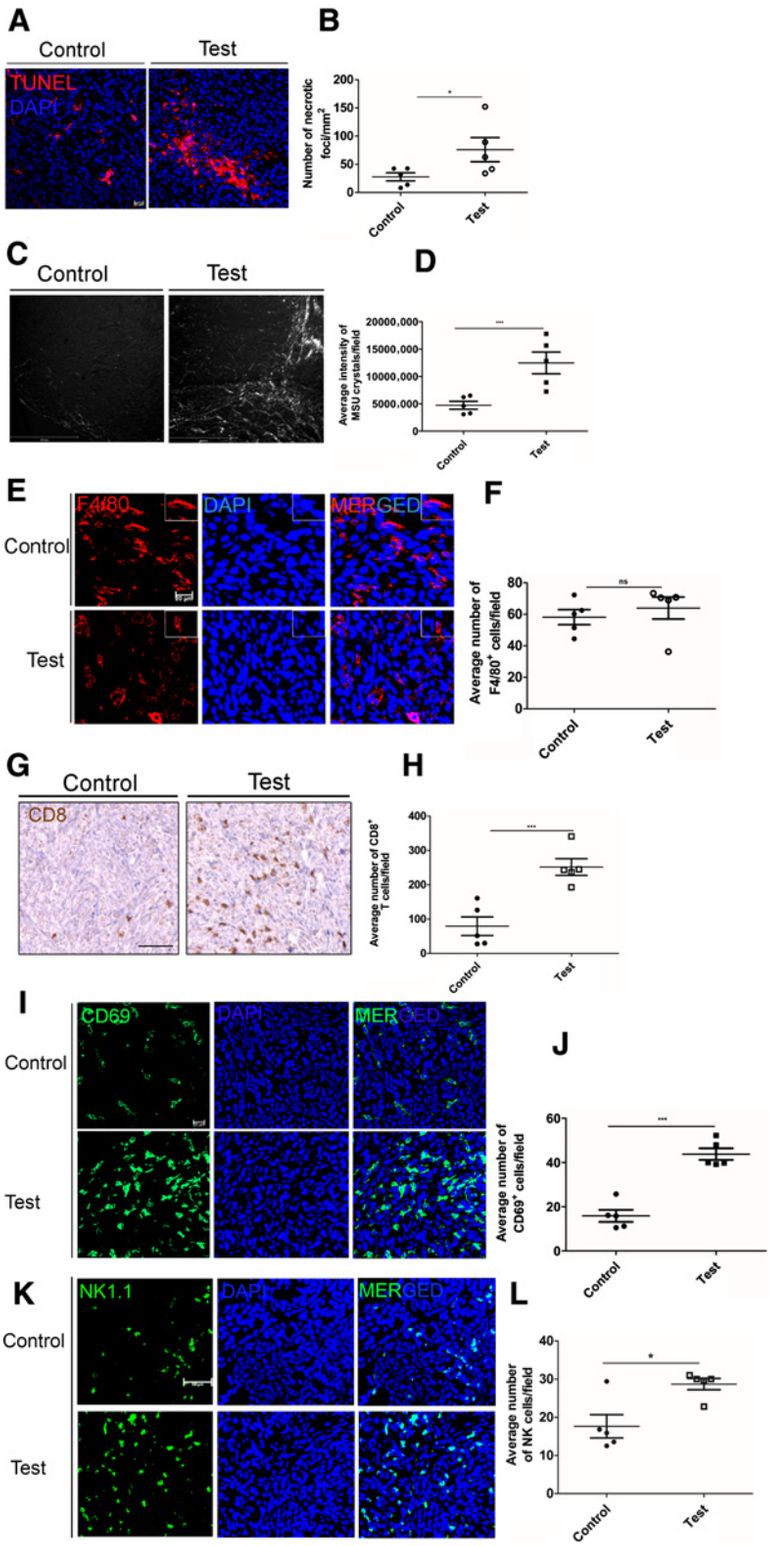

Figure 6.

NRP2 in TAMs regulates the efferocytosis of apoptotic tumor cells and immune responses. **A,** Representative image showing TUNEL$^+$ cells in control and test tumors. **B,** The number of necrotic foci relative to tumor volume shown graphically. **C,** Representative images showing deposition of MSU crystals in control and test tumors. Scale bar, 500 μm. **D,** Scatter plot comparing the formation of MSU crystals in control versus test tumors. **E,** Representative image showing role of NRP2 in the migration of macrophages (F4/80$^+$; red) to the tumor. Scale bar, 20 μm. The inset shows a magnified image of a single F4/80$^+$ macrophage. **F,** The number of F4/80$^+$ cells per field was counted using ImageJ software and represented graphically. **G,** Representative IHC image showing CD8$^+$ T-cell infiltration in control and test tumors. Image scale, ×20 magnification. **H,** Number of CD8$^+$ T cells per field was counted using ImageJ software and is represented graphically. **I,** Representative confocal microscopy image for CD69$^+$ T-cell infiltration (green) in the control and test tumors. Scale bar, 20 μm. **J,** The number of CD69$^+$ T cells per field was counted using ImageJ software and is represented as a scatter plot. **K,** Representative confocal microscopy image for NK1.1$^+$ cells (green) in control and test tumors. Scale bar, 20 μm. **L,** The number of NK1.1$^+$ cells per field was counted using ImageJ software and is represented graphically. DAPI was used to stain the nucleus. All values are mean ± SEM. *, $P < 0.05$; ***, $P < 0.0005$; ns, not significant.

macrophages act synergistically and result in a robust infiltration of CD8$^+$ T and NK cells into the tumors and impede tumor growth.

Discussion

Limited information is currently available about the role of NRP2 in macrophages. Our results indicated that NRP2 is

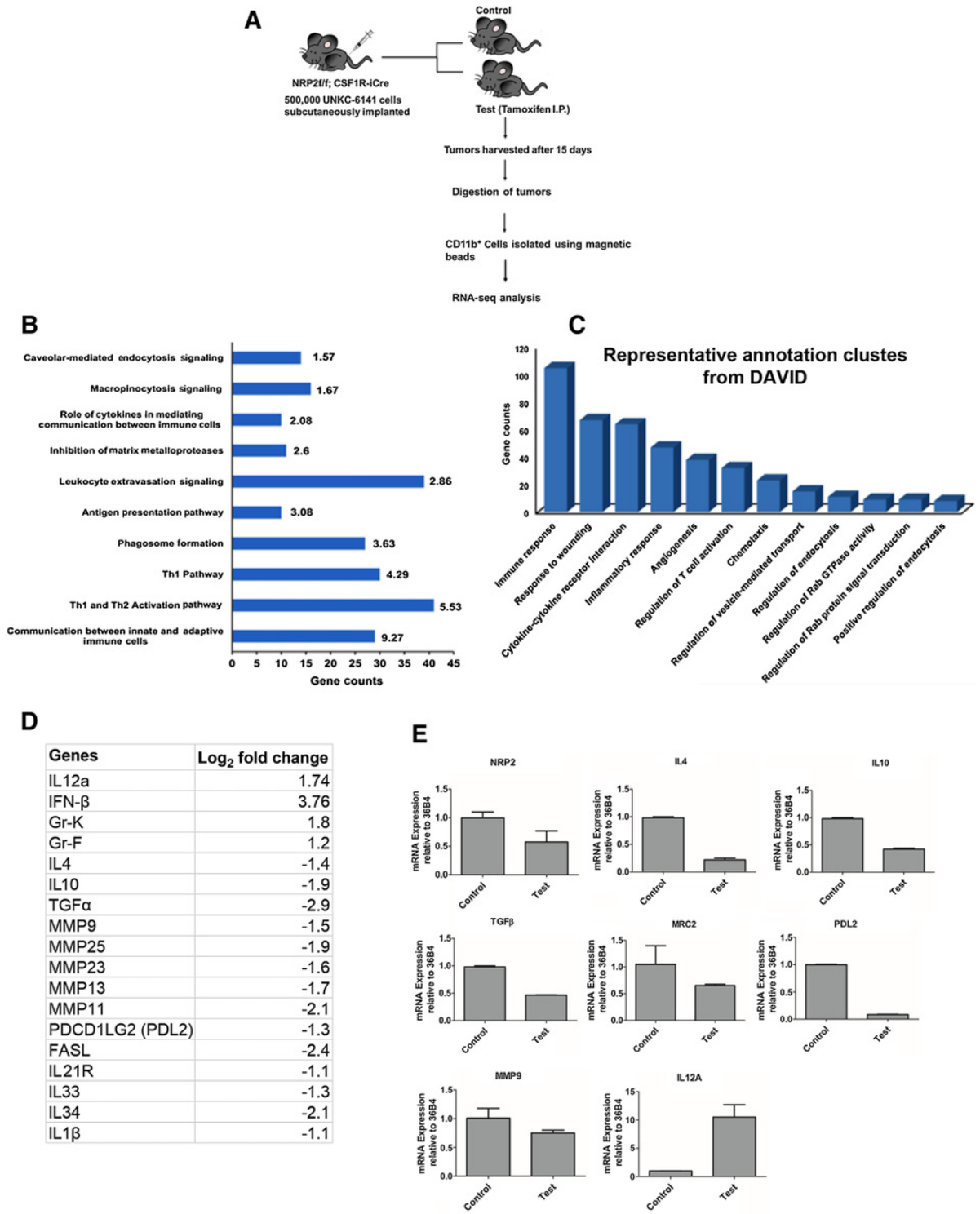

Genes	Log_2 fold change
IL12a	1.74
IFN-β	3.76
Gr-K	1.8
Gr-F	1.2
IL4	-1.4
IL10	-1.9
TGFα	-2.9
MMP9	-1.5
MMP25	-1.9
MMP23	-1.6
MMP13	-1.7
MMP11	-2.1
PDCD1LG2 (PDL2)	-1.3
FASL	-2.4
IL21R	-1.1
IL33	-1.3
IL34	-2.1
IL1β	-1.1

Figure 7.

Transcriptome analysis from CD11b$^+$ myeloid cells by next-generation RNA-seq. **A,** Schematic diagram showing experimental design. **B,** Representative canonical pathways from Ingenuity Pathway Analysis are shown with gene counts and $-\log(P)$. **C,** Representative functional annotation clusters from the DAVID database are shown. **D,** Representative list of genes related to macrophage polarization whose expressions were significantly altered in the CD11b$^+$ myeloid population following NRP2 deletion in macrophages in test tumors. **E,** RT-PCR analysis in separate biological replicates (pooled, $n = 3$ in either control or test) showing altered expression of genes in CD11b$^+$ cells following NRP2 deletion in macrophages in test tumors.

expressed during the differentiation of classic and alternatively activated type macrophages. Interestingly, tumor-secreted factors are also capable of inducing NRP2 expression in macrophages. These observations have raised the question what are the potential function(s) of NRP2, which is not only required in normal physiology but may also play a role in pathologic conditions such as cancer. One particularly important question in this context is whether the expression of NRP2 in macrophages present in a tumor is a host response due to the presence of tumor and thus antitumorigenic or its expression in macrophages facilitates tumor growth. The finding would be significant especially in the context of pancreatic cancer, where we detected $NRP2^+$ macrophages in human pancreatic cancer tissues. Studies have indicated potent antitumor effect for drugs that can modulate TAMs in pancreatic cancer to classic inflammatory type (4, 43). We were therefore interested in understanding whether the presence of $NRP2^+$ macrophages in pancreatic tumor microenvironment has a tumor-promoting or tumor-inhibiting function.

Our results presented in this study have answered some of these important questions. We have identified a novel function of NRP2 in macrophages, which is its ability to regulate phagocytosis. We observed a significantly delayed phagosome maturation and degradation of phagocytic cargo in macrophages following NRP2 deletion. Earlier literature suggested that neuropilins influence cellular locomotion. Interestingly, recent report also indicated the presence of a specific polysialylated form of NRP2 in dendritic cells, which is required for their movement to lymph nodes (44). Although NRP2 can potentially promote the migration, studying its other important functions will be crucial for the comprehensive understanding of its role in macrophages and how it can be targeted for the development of novel therapies against aggressive malignancy. In this respect, our finding that NRP2 regulates the phagocytic activity of macrophages is significant. We speculate that the regulation of phagocytic activity is dominantly regulated by NRP2. Although as discussed in the Results section, it is difficult to rule out the possibility that NRP1 may also regulate phagocytosis in macrophages albeit with lesser efficiency. Interestingly, there are some reports where the authors have shown Tuftsin promoted phagocytosis in microglia in an NRP1-dependent manner (45). This needs to be tested in future studies using a mouse model where NRP1 can be genetically deleted.

To further understand how NRP2 regulates the phagocytic activity of macrophages, we tested whether NRP2 knockdown or deletion leads to a defect in the uptake of phagocytic cargo or delays the maturation of phagosomes. Our experiments indicated that NRP2 knockdown or deletion did not result in any significant decrease in the uptake of phagocytic cargo and suggested a defect in the maturation processes. A conclusive proof for the involvement of NRP2 in regulating the maturation process of phagosomes came when we observed an increase in $Rab5^+$ early vesicles with a concomitant decrease in $Rab7^+$ late vesicles following NRP2 knockdown or deletion, suggesting a defect during the exchange of Rab5 to Rab7 in phagosomes. Generation of $Rab7^+$ phagosomes is crucial for phagosome maturation and is a prerequisite step for phagosomes during their fusion with lysosomes to form phagolysosomes (33, 34, 46–49). We therefore concluded that the molecular effectors downstream of Rab5 are regulated by the NRP2 axis to promote fusion between phagosome and lysosome. This is what we have observed for zymosan and apoptotic cells, where deletion of NRP2 resulted in a significant delay in cargo degradation, indicating a problem in lysosome fusion during phagosome maturation. We also noticed that for apoptotic cells and zymosan, the pH-sensitive dye fluorescence increased within 30 or 60 minutes, respectively, of adding the phagocytic cargo to macrophages (Supplementary Fig. S4A and S4B), which was significantly shorter than what we observed for *E. coli* particle (~90 minutes). This could be either due to faster time for maturation of apoptotic cell and zymosan-containing phagosomes or due to more acidic environment in those phagosomes even when they were in their earlier stages of maturation. Nevertheless, there was no detectable change in maturation kinetics for apoptotic cell (Supplementary Fig. S4C) and zymosan (Supplementary Fig. S4F) containing phagosomes in NRP2-KO versus control macrophages, thus indicating that NRP2 is not involved during their early maturation. However, the dye intensity for *E. coli* containing phagosomes did not reach its peak even after 4 hours of chase, suggesting a maturation defect that could happen earlier than Rab5–Rab7 exchange during phagosome maturation. Currently, it is unknown whether NRP2 can regulate any other steps of phagosome maturation when *E. coli* particle is phagocytized. Interestingly, by carefully analyzing the expression pattern of genes detected by IPA (canonical pathway: phagosome formation) and DAVID (annotation clusters 91 and 92) as well as additional genes from our RNA-seq data set, we have identified some potential molecular mediators of phagosome maturation process. We detected altered expression of several genes belonging to the Rab family of proteins following NRP2 deletion in macrophages, including those associated with phagocytosis or maturation such as *Tubb4a*, *TubA8*, and *Rufy4a*. One microRNA, miR-24 was significantly upregulated in NRP2-deleted TAMs. This miRNA has been reported to attenuate phagocytosis as well modulate inflammatory cytokines in macrophages and DCs (50–53). The contribution of these NRP2-regulated genes in the phagosome maturation and degradation of different cargo is currently unknown and merits further investigation. Also, because macropinocytosis and phagocytosis are similar in many aspects, especially during their maturation, NRP2 may regulate macropinocytosis as well. The conditions we chose for our experiments predominantly favor phagosome formation, although it did not rule out the possibility that in other conditions NRP2 regulates maturation of macropinosomes and thus control some important biological functions.

One of the most important functions of macrophages is the efferocytic clearance of apoptotic cells in an immunologically silent manner. Efferocytosis generates soluble and cell-bound signals that result in an anti-inflammatory state necessary for immune homeostasis (14). Under conditions of impaired efferocytosis, apoptotic cells undergo secondary necrosis releasing an array of cell-derived factors that can potentially activate immune responses and result in autoimmunity and lupus like conditions. Our *in vitro* assay with apoptotic cells suggested a role of NRP2 in regulating efferocytosis in macrophages. Deletion of NRP2 significantly delayed the degradation of apoptotic cells in the macrophages. Emerging evidence now suggests a potential protumoral role of efferocytosis in tumor progression and metastases (17). Efferocytosis by TAMs is potentially tumorigenic as it induces excessive protumorigenic polarization and production of wound healing and immunosuppressive cytokines. This helps suppress antitumor adaptive responses and actively support tumor growth. In this respect, it is important to note that radiation or chemotherapy induced

apoptosis in tumor cells triggers defective repair macrophages and thus activates a vicious feed-forward loop for cancer progression. We therefore hypothesized that deletion of NRP2 in macrophages in a tumor microenvironment can hinder their ability to phagocytose dying tumor cells, which should lead to an increase in secondary necrosis and thus a reduction in tumor growth. Indeed, deleting NRP2 from macrophages in mice bearing subcutaneous pancreatic tumors significantly impaired their efferocytic activity and increased secondary necrosis in the tumors. This reinitiated an antitumor immunogenic response characterized by a robust infiltration of active $CD8^+$ T and NK cells into the tumors following NRP2 deletion in TAMs and reduced tumor growth. Although reports have documented a role for NRP1 in inducing a protumorigenic phenotype in macrophages (25, 26), its role in efferocytosis has not been studied. As previously mentioned, future studies with NRP1 KO mice will answer this interesting question.

Efferocytosis promotes an immunosuppressive microenvironment by cellular mechanisms not completely understood. The release of cellular contents from a secondary necrotic cell in the extracellular milieu in the absence of efferocytosis induces antitumor immune responses. Indeed, we observed a significant infiltration of $CD8^+$ T and NK cells along with inhibition of growth in test tumors, suggesting an antitumor immune response. Delayed efferocytosis could also suppress the expression of immunosuppressive genes in macrophages and activate immunogenic responses (12, 14, 54). Indeed, our RNA-seq analysis in NRP2-deleted myeloid cells indicated additional changes in gene signatures for enhanced $CD8^+$ T and NK cell activation and reduced tumor growth. We identified suppression of several wound healing and immunosuppressive genes that can support tumor-promoting TAM phenotype or recruit and activate Tregs or blunt T and NK cell activation, whereas inflammatory genes or those with immune stimulatory potential were upregulated in NRP2-deleted condition. Taken together, we conclude that NRP2 deletion in macrophages affects a wide array of molecules associated with the immune response in the myeloid compartment that act in consort and result in robust $CD8^+$ T and NK cell responses.

The expansion and recruitment of antitumor immune cells of adaptive or innate arms to the tumor microenvironment can significantly control tumor growth. This has been exemplified by the recent demonstration that administration of anti-CD40 antibody resulted in the mobilization of tumor-killing peripheral macrophages in pancreatic tumors (55). We speculate that NRP2-expressing TAMs due to their high efferocytic activity are immunosuppressive and therefore actively promote tumor progression. It is plausible that NRP2-driven efferocytosis of apoptotic tumor cells is a major contributing factor for the failure of cytotoxic therapies, which causes widespread apoptotic tumor cell death. Because therapy-induced tumor cell apoptosis will increase efferocytosis, we speculate it will further exaggerate the immune suppressive microenvironment and result in more aggressive tumors with higher metastatic potential. Thus, inhibiting the NRP2 axis in TAMs would reduce pancreatic tumor progression and enhance the efficacy of established treatment modalities when used in combination with either chemotherapy or other immunotherapies.

Disclosure of Potential Conflicts of Interest

No potential conflicts of interest were disclosed.

Authors' Contributions

Conception and design: S. Roy, A.K. Bag, S. Dutta, S. Ran, M.A. Hollingsworth, M.H. Muders, S.K. Batra, K. Datta
Development of methodology: S. Roy, A.K. Bag, S. Dutta, N.S. Polavaram, K. Datta
Acquisition of data (provided animals, acquired and managed patients, provided facilities, etc.): S. Roy, A.K. Bag, N.S. Polavaram, R. Islam
Analysis and interpretation of data (e.g., statistical analysis, biostatistics, computational analysis): S. Roy, A.K. Bag, J. Banwait, C. Guda, R.K. Singh, J.E. Talmadge, K. Datta
Writing, review, and/or revision of the manuscript: S. Roy, A.K. Bag, R. Islam, S. Schellenburg, C. Guda, S. Ran, M.A. Hollingsworth, R.K. Singh, J.E. Talmadge, M.H. Muders, S.K. Batra, K. Datta
Administrative, technical, or material support (i.e., reporting or organizing data, constructing databases): S. Roy, A.K. Bag, K. Datta
Study supervision: S. Roy, S. Dutta, K. Datta

Acknowledgments

The authors thank Karen Yip and the team at Seqmatic (via Science Exchange) for the RNA-seq services, Janice A. Taylor and James R. Talaska at the Confocal Laser Scanning Microscope Core Facility, Victoria Smith and Samantha Wall at the Flow Cytometry facility and the animal care facility at the University of Nebraska Medical Center for their assistance, Fred and Pamela Buffet Cancer Center Shared Resources, supported by NCI under award number P30CA036727, and Dr. Paul Grandgenett of the RAP program at UNMC for providing the PDAC tissues.

The study was supported by R01-NIH 1R01CA182435-01A1, The Nebraska Center for Cellular Signaling CoBRE Developmental Grant P30 GM106397, Pancreatic Tumor Microenvironment Network (TMEN) U54CA163120-03, Pancreas SPORE Developmental Research Program 2013 RFA, UNMC P50 CA127297, Fred and Pamela Buffet Cancer Center Support Grant from NCI (P30CA036727), German Research Foundation DFG (grant MU2687/5-1), and Rudolf Becker Foundation for Prostate Cancer Research.

The costs of publication of this article were defrayed in part by the payment of page charges. This article must therefore be hereby marked *advertisement* in accordance with 18 U.S.C. Section 1734 solely to indicate this fact.

Received February 22, 2018; revised June 6, 2018; accepted August 7, 2018; published first August 15, 2018.

References

1. Okabe Y, Medzhitov R. Wormhole travel for macrophages. Cell 2016; 165:518–9.
2. Mosser DM, Edwards JP. Exploring the full spectrum of macrophage activation. Nat Rev Immunol 2008;8:958–69.
3. Martinez FO, Gordon S. The M1 and M2 paradigm of macrophage activation: time for reassessment. F1000Prime Rep 2014;6:13.
4. Mantovani A, Marchesi F, Malesci A, Laghi L, Allavena P. Tumour-associated macrophages as treatment targets in oncology. Nat Rev Clin Oncol 2017;14:399–416.
5. Noy R, Pollard JW. Tumor-associated macrophages: from mechanisms to therapy. Immunity 2014;41:49–61.
6. Elliott MR, Ravichandran KS. Clearance of apoptotic cells: implications in health and disease. J Cell Biol 2010;189:1059–70.
7. Ravichandran KS. Find-me and eat-me signals in apoptotic cell clearance: progress and conundrums. J Exp Med 2010;207:1807–17.
8. Franz S, Gaipl US, Munoz LE, Sheriff A, Beer A, Kalden JR, et al. Apoptosis and autoimmunity: when apoptotic cells break their silence. Curr Rheumatol Rep 2006;8:245–7.

9. Baumann I, Kolowos W, Voll RE, Manger B, Gaipl U, Neuhuber WL, et al. Impaired uptake of apoptotic cells into tingible body macrophages in germinal centers of patients with systemic lupus erythematosus. Arthritis Rheum 2002;46:191–201.
10. Munoz LE, Janko C, Chaurio RA, Schett G, Gaipl US, Herrmann M. IgG opsonized nuclear remnants from dead cells cause systemic inflammation in SLE. Autoimmunity 2010;43:232–5.
11. Munoz LE, Janko C, Schulze C, Schorn C, Sarter K, Schett G, et al. Autoimmunity and chronic inflammation - two clearance-related steps in the etiopathogenesis of SLE. Autoimmun Rev 2010;10:38–42.
12. Munoz LE, Lauber K, Schiller M, Manfredi AA, Herrmann M. The role of defective clearance of apoptotic cells in systemic autoimmunity. Nat Rev Rheumatol 2010;6:280–9.
13. Munoz LE, Lauber K, Schiller M, Manfredi AA, Schett G, Voll RE, et al. [The role of incomplete clearance of apoptotic cells in the etiology and pathogenesis of SLE]. Z Rheumatol 2010;69:152, 4–6.
14. Henson PM. Cell removal: efferocytosis. Annu Rev Cell Dev Biol 2017;33: 127–44.
15. Fadok VA, Bratton DL, Guthrie L, Henson PM. Differential effects of apoptotic versus lysed cells on macrophage production of cytokines: role of proteases. J Immunol 2001;166:6847–54.
16. Green DR, Ferguson T, Zitvogel L, Kroemer G. Immunogenic and tolerogenic cell death. Nat Rev Immunol 2009;9:353–63.
17. Stanford JC, Young C, Hicks D, Owens P, Williams A, Vaught DB, et al. Efferocytosis produces a prometastatic landscape during postpartum mammary gland involution. J Clin Invest 2014;124:4737–52.
18. Kumar S, Calianese D, Birge RB. Efferocytosis of dying cells differentially modulate immunological outcomes in tumor microenvironment. Immunol Rev 2017;280:149–64.
19. Birge RB, Boeltz S, Kumar S, Carlson J, Wanderley J, Calianese D, et al. Phosphatidylserine is a global immunosuppressive signal in efferocytosis, infectious disease, and cancer. Cell Death Differ 2016;23:962–78.
20. Cook RS, Jacobsen KM, Wofford AM, DeRyckere D, Stanford J, Prieto AL, et al. MerTK inhibition in tumor leukocytes decreases tumor growth and metastasis. J Clin Invest 2013;123:3231–42.
21. Chen X, Doffek K, Sugg SL, Shilyansky J. Phosphatidylserine regulates the maturation of human dendritic cells. J Immunol 2004;173:2985–94.
22. Roca H, Jones JD, Purica MC, Weidner S, Koh AJ, Kuo R, et al. Apoptosis-induced CXCL5 accelerates inflammation and growth of prostate tumor metastases in bone. J Clin Invest 2018;128:248–66.
23. Casazza A, Laoui D, Wenes M, Rizzolio S, Bassani N, Mambretti M, et al. Impeding macrophage entry into hypoxic tumor areas by Sema3A/Nrp1 signaling blockade inhibits angiogenesis and restores antitumor immunity. Cancer Cell 2013;24:695–709.
24. Dai X, Okon I, Liu Z, Wu Y, Zhu H, Song P, et al. A novel role for myeloid cell-specific neuropilin 1 in mitigating sepsis. FASEB J 2017;31:2881–92.
25. Miyauchi JT, Caponegro MD, Chen D, Choi MK, Li M, Tsirka SE. Deletion of Neuropilin 1 from microglia or bone marrow-derived macrophages slows glioma progression. Cancer research 2018;78:685–94.
26. Miyauchi JT, Chen D, Choi M, Nissen JC, Shroyer KR, Djordevic S, et al. Ablation of Neuropilin 1 from glioma-associated microglia and macrophages slows tumor progression. Oncotarget 2016;7:9801–14.
27. Roy S, Bag AK, Singh RK, Talmadge JE, Batra SK, Datta K. Multifaceted role of neuropilins in the immune system: potential targets for immunotherapy. Front Immunol 2017;8:1228.
28. Walz A, Rodriguez I, Mombaerts P. Aberrant sensory innervation of the olfactory bulb in neuropilin-2 mutant mice. J Neurosci 2002;22:4025–35.
29. Mielgo A, Schmid MC. Impact of tumour associated macrophages in pancreatic cancer. BMB Rep 2013;46:131–8.
30. Protti MP, De Monte L. Immune infiltrates as predictive markers of survival in pancreatic cancer patients. Front Physiol 2013;4:210.
31. Gordon S. Phagocytosis: an immunobiologic process. Immunity 2016; 44:463–75.
32. Martinez J, Cunha LD, Park S, Yang M, Lu Q, Orchard R, et al. Noncanonical autophagy inhibits the autoinflammatory, lupus-like response to dying cells. Nature 2016;533:115–9.
33. Kinchen JM, Ravichandran KS. Phagosome maturation: going through the acid test. Nat Rev Mol Cell Biol 2008;9:781–95.
34. Hochreiter-Hufford A, Ravichandran KS. Clearing the dead: apoptotic cell sensing, recognition, engulfment, and digestion. Cold Spring Harb Perspect Biol 2013;5:a008748.
35. Pesce J, Kaviratne M, Ramalingam TR, Thompson RW, Urban JF Jr, Cheever AW, et al. The IL-21 receptor augments Th2 effector function and alternative macrophage activation. J Clin Invest 2006;116:2044–55.
36. Zhang Y, Davis C, Shah S, Hughes D, Ryan JC, Altomare D, et al. IL-33 promotes growth and liver metastasis of colorectal cancer in mice by remodeling the tumor microenvironment and inducing angiogenesis. Mol Carcinog 2017;56:272–87.
37. Segaliny AI, Mohamadi A, Dizier B, Lokajczyk A, Brion R, Lanel R, et al. Interleukin-34 promotes tumor progression and metastatic process in osteosarcoma through induction of angiogenesis and macrophage recruitment. Int J Cancer 2015;137:73–85.
38. Li Y, Wang L, Pappan L, Galliher-Beckley A, Shi J. IL-1beta promotes stemness and invasiveness of colon cancer cells through Zeb1 activation. Mol Cancer 2012;11:87.
39. Li CW, Xia W, Huo L, Lim SO, Wu Y, Hsu JL, et al. Epithelial-mesenchymal transition induced by TNF-alpha requires NF-kappaB-mediated transcriptional upregulation of Twist1. Cancer Res 2012;72:1290–300.
40. Gialeli C, Theocharis AD, Karamanos NK. Roles of matrix metalloproteinases in cancer progression and their pharmacological targeting. FEBS J 2011;278:16–27.
41. Cathcart J, Pulkoski-Gross A, Cao J. Targeting matrix metalloproteinases in cancer: bringing new life to old ideas. Genes Dis 2015;2:26–34.
42. Shay G, Lynch CC, Fingleton B. Moving targets: Emerging roles for MMPs in cancer progression and metastasis. Matrix Biol 2015; 44–46:200–6.
43. Thind K, Padrnos LJ, Ramanathan RK, Borad MJ. Immunotherapy in pancreatic cancer treatment: a new frontier. Therap Adv Gastroenterol 2017;10:168–94.
44. Rey-Gallardo A, Escribano C, Delgado-Martin C, Rodriguez-Fernandez JL, Gerardy-Schahn R, Rutishauser U, et al. Polysialylated neuropilin-2 enhances human dendritic cell migration through the basic C-terminal region of CCL21. Glycobiology 2010;20:1139–46.
45. Nissen JC, Tsirka SE. Tuftsin-driven experimental autoimmune encephalomyelitis recovery requires neuropilin-1. Glia 2016;64:923–36.
46. Kitano M, Nakaya M, Nakamura T, Nagata S, Matsuda M. Imaging of Rab5 activity identifies essential regulators for phagosome maturation. Nature 2008;453:241–5.
47. Arandjelovic S, Ravichandran KS. Phagocytosis of apoptotic cells in homeostasis. Nat Immunol 2015;16:907–17.
48. Kinchen JM, Doukoumetzidis K, Almendinger J, Stergiou L, Tosello-Trampont A, Sifri CD, et al. A pathway for phagosome maturation during engulfment of apoptotic cells. Nat Cell Biol 2008;10:556–66.
49. Kinchen JM, Ravichandran KS. Identification of two evolutionarily conserved genes regulating processing of engulfed apoptotic cells. Nature 2010;464:778–82.
50. Fordham JB, Naqvi AR, Nares S. miR-24 Regulates Macrophage Polarization and Plasticity. J Clin Cell Immunol 2015;6:362.
51. Fordham JB, Naqvi AR, Nares S. Regulation of miR-24, miR-30b, and miR-142-3p during macrophage and dendritic cell differentiation potentiates innate immunity. J Leukoc Biol 2015;98:195–207.
52. Naqvi AR, Fordham JB, Ganesh B, Nares S. miR-24, miR-30b and miR-142-3p interfere with antigen processing and presentation by primary macrophages and dendritic cells. Sci Rep 2016;6:32925.
53. Naqvi AR, Fordham JB, Nares S. miR-24, miR-30b, and miR-142-3p regulate phagocytosis in myeloid inflammatory cells. J Immunol 2015; 194:1916–27.
54. Henson PM, Bratton DL, Fadok VA. Apoptotic cell removal. Curr Biol 2001;11:R795–805.
55. Vonderheide RH, Bajor DL, Winograd R, Evans RA, Bayne LJ, Beatty GL. CD40 immunotherapy for pancreatic cancer. Cancer Immunol Immunother 2013;62:949–54.